AMERICAN SOCIETY FOR MICROBIOLOGY | Journal of Virology

Alpha-Synuclein Expression Restricts RNA Viral Infections in the Brain

Erica L. Beatman,[a] Aaron Massey,[a] Katherine D. Shives,[a,c] Kristina S. Burrack,[c]* Mastooreh Chamanian,[a] Thomas E. Morrison,[c] J. David Beckham[a,b,c]

Department of Medicine, Division of Infectious Diseases,[a] Department of Neurology,[b] and Department of Immunology & Microbiology,[c] University of Colorado School of Medicine, Aurora, Colorado, USA

ABSTRACT

We have discovered that native, neuronal expression of alpha-synuclein (Asyn) inhibits viral infection, injury, and disease in the central nervous system (CNS). Enveloped RNA viruses, such as West Nile virus (WNV), invade the CNS and cause encephalitis, yet little is known about the innate neuron-specific inhibitors of viral infections in the CNS. Following WNV infection of primary neurons, we found that Asyn protein expression is increased. The infectious titer of WNV and Venezuelan equine encephalitis virus (VEEV) TC83 in the brains of Asyn-knockout mice exhibited a mean increase of $10^{4.5}$ infectious viral particles compared to the titers in wild-type and heterozygote littermates. Asyn-knockout mice also exhibited significantly increased virus-induced mortality compared to Asyn heterozygote or homozygote control mice. Virus-induced Asyn localized to perinuclear, neuronal regions expressing viral envelope protein and the endoplasmic reticulum (ER)-associated trafficking protein Rab1. In Asyn-knockout primary neuronal cultures, the levels of expression of ER signaling pathways, known to support WNV replication, were significantly elevated before and during viral infection compared to those in Asyn-expressing primary neuronal cultures. We propose a model in which virus-induced Asyn localizes to ER-derived membranes, modulates virus-induced ER stress signaling, and inhibits viral replication, growth, and injury in the CNS. These data provide a novel and important functional role for the expression of native alpha-synuclein, a protein that is closely associated with the development of Parkinson's disease.

IMPORTANCE

Neuroinvasive viruses such as West Nile virus are able to infect neurons and cause severe disease, such as encephalitis, or infection of brain tissue. Following viral infection in the central nervous system, only select neurons are infected, implying that neurons exhibit innate resistance to viral infections. We discovered that native neuronal expression of alpha-synuclein inhibited viral infection in the central nervous system. When the gene for alpha-synuclein was deleted, mice exhibited significantly decreased survival, markedly increased viral growth in the brain, and evidence of increased neuron injury. Virus-induced alpha-synuclein localized to intracellular neuron membranes, and in the absence of alpha-synuclein expression, specific endoplasmic reticulum stress signaling events were significantly increased. We describe a new neuron-specific inhibitor of viral infections in the central nervous system. Given the importance of alpha-synuclein as a cause of Parkinson's disease, these data also ascribe a novel functional role for the native expression of alpha-synuclein in the CNS.

Viral infections of the central nervous system (CNS) cause significant disease and mortality throughout the world (1, 2) and are likely to have an evolutionary impact on the development of innate neuronal restriction factors in the central nervous system. Herpes simplex virus 1 (HSV-1), for example, is the most common cause of sporadic viral encephalitis in the world (1). Infections of the CNS by RNA viruses, such as West Nile virus (WNV) and Japanese encephalitis virus (JEV), also cause substantial global disease burdens. These viruses infect and injure the subcortical gray matter, such as the basal ganglia, substantia nigra, brain stem, and cerebellum, while they largely spare the cortex (3–6). Some patients with WNV or JEV encephalitis develop Parkinsonian symptoms, such as bradykinesia, tremor, cogwheel rigidity, and wide-based gait (7). Similar Parkinsonian signs and symptoms are associated with a variety of other enveloped RNA virus infections (8, 9). Recent work has shown that innate immune responses to viral infections in the CNS contribute to neuron-specific injury patterns and susceptibility to viral infection (10). However, native expression of a neuron-specific restriction factor for viral infections has not been described.

Parkinson's disease (PD) is the second most common neurodegenerative disorder in the world (11, 12). Evidence increasingly suggests that alpha-synuclein (Asyn) plays a causative role in PD pathogenesis and injury in the substantia nigra of the human brain. Asyn is a major constituent of Lewy bodies (LBs), the hallmark pathological feature of PD and other neurodegenerative disorders referred to as synucleinopathies (13). Missense mutations in the Asyn gene (A53T, A30P, E46K) and duplication of the PD locus (PARK1) cause PD (12, 14–20). Mice expressing transgenic

Received 20 November 2015 **Accepted** 14 December 2015

Accepted manuscript posted online 30 December 2015

Citation Beatman EL, Massey A, Shives KD, Burrack KS, Chamanian M, Morrison TE, Beckham JD. 2016. Alpha-synuclein expression restricts RNA viral infections in the brain. J Virol 90:2767–2782. doi:10.1128/JVI.02949-15.

Editor: S. Perlman

Address correspondence to J. David Beckham, david.beckham@ucdenver.edu.

* Present address: Kristina S. Burrack, Department of Laboratory Medicine and Pathology, University of Minnesota, Minneapolis, Minnesota, USA.

E.L.B. and A.M. are co-first authors and contributed equally to the article.

human Asyn in the brain exhibit neuronal injury patterns similar to those found in patients with PD, implying that native expression of human Asyn and not Lewy body aggregates may play a role in neuronal toxicity (21). Thus, elucidating the functional roles of native Asyn expression in neurons will provide insight into possible mechanisms of injury related to PD.

The mechanism of Asyn-induced toxicity and the function of natively expressed Asyn in neurons are not understood. Mice lacking the gene for Asyn (*Snca*) exhibit normal life spans, normal reproduction, normal neuronal content and number, and normal development (22). Asyn-knockout mice do exhibit an increased release of dopamine with paired stimuli concurrently with a reduction in striatal dopamine and an attenuation of the dopamine-dependent locomotor response to amphetamine (22). Following treatment with (1-methyl-4-phenyl-1,2,3,6-tetrahydropyridine), a pharmacological agent used to induce the experimental loss of dopaminergic neurons, Asyn-knockout mice also exhibit a marked resistance to neurotoxicity (23). These data support the hypothesis that Asyn functions in part as a presynaptic, activity-dependent negative regulator of dopamine neurotransmission. However, the role of native Asyn protein expression in neurons at a basal state is not understood, and the reason why Asyn is nearly exclusively expressed in neurons is not known.

Recent data show that native expression of Asyn alters intra- and interneuronal vesicle transport through interactions with Rab proteins and soluble *N*-ethylmaleimide-sensitive factor attachment protein receptor (SNARE) complexes (24, 25). The N terminus of native Asyn contains seven, 11-residue repeats that form an amphipathic alpha-helix and interact directly with the surface of lipid membranes (26). Point mutations in Asyn (A53T, A30P, E46K) that are associated with familial inherited forms of PD are relegated to the N-terminal domain that associates with membranes (17, 20). Asyn is thought to maintain a homeostatic balance between cytosolic, randomly folded monomers and lipid membrane-associated multimers that associate with Rab and SNARE proteins in the exocytosis pathway through interactions at the C terminus of the Asyn protein (24, 25). In particular, Asyn associates with Rab1-expressing ($Rab1^+$) endoplasmic reticulum (ER)-Golgi body transport vesicles (27). When Asyn is localized to ER-Golgi body transport vesicles, it prevents docking to the Golgi body and alters ER stress signaling. The underlying physiological purpose of this regulatory link between the alteration in ER-Golgi vesicle trafficking and the modulation of ER stress signaling is not known. Thus, we defined the role of Asyn during viral infection of the CNS since many neuroinvasive viruses cause Parkinsonian symptoms and require extensive interactions with the neuronal membrane systems for replication and growth.

We have discovered that native Asyn expression in neurons inhibits viral growth and injury in the CNS. We also show that virus-induced Asyn expression in neurons localizes with $Rab1^+$ membrane compartments, and in the absence of Asyn, ER stress signaling is significantly altered, resulting in activation of the signaling pathway known to support viral replication and contribute to virus-induced apoptosis.

MATERIALS AND METHODS

Ethics statement. Animal work was done in accordance with and following approval by Institutional Animal Care and Use Committee (IACUC) guidelines at the University of Colorado Denver Anschutz Medical Campus. University of Colorado Health Sciences Center Animal Care and Use Committee protocol number B88815(06)1E was reapproved on 4 June 2015. The animal protocol was written and approved to be in compliance with the *Guide for the Care and Use of Laboratory Animals* of the National Research Council's Institute for Laboratory Animal Research (28), the Animal Welfare Act, the USDA Animal Care Policy, and PHS/NIH/OLAW policy. The protocol adheres to AVMA guidelines on euthanasia. Euthanasia of animals was done by approved mechanisms, such as CO_2 inhalation, isoflurane overdose, and secondary methods, including cervical dislocation. The University of Colorado Institutional Biosafety Committee reviewed and approved all work with live viruses and recombinant DNA in accordance with local and national regulations of pathogens. Human brain tissue was obtained from deidentified human autopsy cases at the University of Colorado Hospital, and research with that material was reviewed and approved as nonhuman exempt research by the Colorado Multiple Institutional Review Board (COMIRB).

Virus propagation, viral titer analysis, and cell lines. West Nile virus stocks were obtained from clone-derived strain 385-99 (NY99) and propagated in C6/36 *Aedes albopictus* (ATCC CRL-1660) cells as previously described (29). Syrian golden hamster kidney cells (BHK-21; ATCC C-13) were used to measure the viral titer by a standard plaque assay as described previously (29). For infection, cells were inoculated with WNV and incubated at 37°C in 5% CO_2 for 1 h in 0.5 ml of basal medium. Venezuelan equine encephalitis virus (VEEV) TC83 isolates were obtained from Michael Diamond's laboratory. Virus was propagated in Vero cells (CCL-81; ATCC), and the viral titer was obtained as previously described (29).

All cell lines were maintained at 37°C in 5% CO_2. Vero (ATCC CCL-81) and BHK-21 cells were maintained in minimum essential medium containing Earle's salts and L-glutamine supplemented with 1% penicillin-streptomycin, 10% heat-inactivated fetal bovine serum, 1% nonessential amino acids, and 1% sodium pyruvate. Human embryonic kidney 293T (HEK293T) cells (ATCC CRL-3216) were maintained in Dulbecco's modified Eagle medium supplemented with 1% penicillin-streptomycin, 10% heat-inactivated fetal bovine serum, 1% HEPES, and 1% sodium pyruvate.

Primary neuronal culture generation. The generation of primary neuronal cultures has been described at length elsewhere (29). In brief, pregnant Swiss Webster mice (Harlan Laboratories), C57BL/6 mice, or $Snca^{-/-}$ mice were euthanized in accordance with University of Colorado Office of Laboratory Animal Research- and IACUC-approved protocols. Brain tissue from embryonic (embryonic day 15) mice was dissected to isolate striatal tissue and parietal cortical tissue. Brain tissues were placed in Ca^{2+}- and Mg^{2+}-free Hanks balanced salt solution with 10 mM HEPES. The tissues were minced with a razor blade and treated with 0.25% trypsin (Sigma-Aldrich) for 30 min and 3 mg/ml DNase I (Sigma-Aldrich) for 5 min at 37°C. After the neurons were pelleted by centrifugation at 1,000 × *g* for 5 min and suspended in neuronal plating medium (1× minimum essential medium with Earle's salts, 10 mM HEPES, 10 mM sodium pyruvate, 0.5 mM glutamine, 10% newborn calf serum, 0.6% glucose, 2% B27 supplement (Gibco), 1% penicillin-streptomycin), they were counted and plated in neuronal plating medium on poly-D-lysine-coated plates. Striatal tissue cultures were generated as a 2:3 coculture of striatal tissue to cortical neurons. At 24 h postplating, the medium was removed and exchanged with glial cell conditioned medium (neurobasal medium supplemented with 2% B27 and 2.5% glutamine). Neuronal cultures were then allowed 6 days to mature prior to infection.

WB analysis. Whole-cell lysate preparation and Western blot (WB) analysis were performed as previously described (29, 30). Cells were suspended in lysis buffer consisting of 1% Triton X-100, 10 mM triethanolamine-HCl, 150 mM NaCl, 5 mM EDTA, 1× Halt protease, and phosphatase inhibitor cocktail (Thermo Scientific, Rockford, IL) and disrupted using an ultrasonic processor (VCX130; Sonics & Materials). Whole-cell extracts were run on standard SDS-polyacrylamide gels (Criterion system; Bio-Rad, USA). The separated proteins were electrically transferred to 0.2-μm-pore-size polyvinylidene fluoride membranes (Millipore, USA). For all WB analyses, membranes were activated for 10

to 15 s in methanol and blocked for 1 h posttransfer with 5% blocking-grade buffer (Bio-Rad). The primary antibodies used for analysis included mouse monoclonal antibody to the WNV envelope (Env; E18 clone; catalog number VR-1611; ATCC), polyclonal rabbit antibody to cleaved caspase-3 (CC3; catalog number 9661S; Cell Signaling Technology [CST]), polyclonal rabbit antibody to alpha-synuclein (catalog number sc-7011-R from Santa Cruz Biotechnology or catalog number 2642 from CST, rabbit monoclonal antibody to protein kinase RNA-like endoplasmic reticulum kinase (PERK; CST), rabbit monoclonal antibody to the α subunit of eukaryotic initiation factor 2 (eIF2α; catalog number 5324; CST), rabbit monoclonal antibody to Ser51 phospho-eIF2α (catalog number 3597; CST), and β-actin (catalog number 4970; CST).

For immunocytofluorescence, images were acquired on an Olympus FV1000 confocal microscope. For immunohistochemistry (IHC) and immunofluorescence (IF) analysis of brain tissue, an Olympus VS120 virtual slide system was used for imaging. Infections were followed as outlined above. Cell counts were completed, using ImageJ software, by an observer that was blinded to the treatment group. For IF analysis, cells of interest were fixed using 4% paraformaldehyde (PFA) in phosphate-buffered saline (PBS) for 10 min. Cells were labeled with primary antibodies, including mouse monoclonal antibody to alpha-synuclein (Cell Signaling Technology and Santa Cruz Biotechnology [catalog number 69977]), rabbit polyclonal antibody to alpha-synuclein (catalog number 7011-R; Santa Cruz Biotechnology), mouse monoclonal antibody to the WNV envelope (E18 clone; ATCC), antibody to double-stranded RNA (a gift from Michael Hall), rabbit polyclonal antibody to Rab1 (Abcam), rabbit polyclonal antibody to Rab5 (Abcam), or rabbit monoclonal antibody to Rab7 (Cell Signaling Technology). Cells were then probed with appropriate fluorescein isothiocyanate (FITC)- or Cy3-conjugated secondary antibodies (Jackson ImmunoResearch, West Grove, PA).

Preparation of mouse and human brain tissue for IF was completed as previously described (31). In addition to being subjected to the standard preparation protocol, all tissue was treated with 0.1% sodium borohydride in PBS prior to antibody labeling to improve antigen unmasking and decrease the background fluorescence of the brain tissue.

Preparation of mouse brain tissue for IHC analysis for CD3 was completed as previously described (31). Additionally, all tissue was treated with 3% hydrogen peroxide in PBS to block endogenous peroxidases. A rabbit monoclonal antibody to CD3 was used to label CD3-positive ($CD3^+$) cells. An anti-rabbit IgG ImmPRESS reagent kit (catalog number MP7401) and ImmPACT NovaRed peroxidase substrate (catalog number SK4805) were purchased from Vector and used for secondary labeling and staining, respectively, according to the manufacturer's protocols.

Chemical cross-linking of Asyn multimers. Cross-linking experiments were performed according to a previously published protocol with modification (25). Cortical and striatal primary neuron preparations were inoculated with WNV (multiplicity of infection [MOI], 1) and isolated as described above at 24 h postadsorption. Neurons were then cross-linked for 5 min at room temperature by adding 50 μl of glutaraldehyde in PBS to achieve final concentrations of 0%, 0.00125%, 0.0025%, or 0.005% for 5 min on the plate before being washed 3 times in ice-cold PBS, scraped, centrifuged and resuspended in lysis buffer containing protease inhibitors. Neuron samples were analyzed by SDS-PAGE and Western blotting. Membranes were probed for alpha-synuclein multimers with a rabbit polyclonal antibody (catalog number 7011-R; Santa Cruz Biotechnology). Rab-GDP dissociation inhibitor (GDI) was used as a marker of the specificity of chemical cross-linking treatment and was probed for with a mouse monoclonal antibody (clone 81.2; Synaptic Systems [SYSY]).

ELISAs. Commercially available enzyme-linked immunosorbent assay (ELISA) kits from R&D Systems were used to determine the concentrations of interferon alpha (IFN-α; catalog number 42400-1), IFN-β (catalog number 42120-1), tumor necrosis factor alpha (TNF-α; catalog number DY410-05), and interleukin-6 (IL-6; catalog number DY406-05) in the cortical and subcortical brain regions of mock- and WNV-infected mice at day 8 postinfection according to the manufacturer's protocols.

WNV RNA qRT-PCR. RNAs were extracted from cells using a Qiagen RNeasy minikit. The quality and quantity of cell-associated RNAs were measured by use of a NanoDrop spectrophotometer. Normalized RNAs were reverse transcribed using SuperScript III reverse transcriptase (Life Technologies) and an oligo(dT) primer (Life Technologies). A Bio-Rad CFX96 real-time system was used for quantitative reverse transcription-PCR (qRT-PCR) amplifications. The 3′ untranslated region of WNV was amplified using the forward primer WNV 3NC F (CAG ACC ACG CTA CGG CG) and the reverse primer WNV 3NC R (CTA GGG CCG CGT GGG) and was detected with probe 6FAM-TCT GCG GAG AGT GCA GTC TGC GAT-MGB-NFQ, where 6FAM is 6-carboxyfluorescein.

***Snca* genotyping.** Normalized amounts of DNA from $Snca^{+/+}$, $Snca^{-/+}$, and $Snca^{-/-}$ mice were used for PCR amplification using Phusion high-fidelity DNA polymerase (NEB). Primers OIMR1286 (GGC GAC GTG AAG GAG CCA GGG A) and OIMR1287 (CAG CGA AAG GAA AGC CGA GTG ATG TAC T) (catalog number 003692; The Jackson Laboratory) were used to amplify the 320-nucleotide (nt) product of the wild-type *Snca* gene. Primers OIMR0158 (CTG AAT GAA CTG CAG GAC GA) and OIMRO159 (ATA CTT TCT CGG CAG GAG CA) were used to amplify the 172-nt product of the *Snca* target gene. The PCR products were detected on a 1% polyacrylamide Tris-acetate-EDTA gel containing ethidium bromide.

Mouse experiments. C57BL/6 breeder mice were obtained from Charles River, and breeder $Snca^{-/-}$ mice were obtained from The Jackson Laboratory (B6; 129X1-$Snca^{tm1Rosl/J}$). $Snca^{-/+}$ mice were bred by crossing male $Snca^{-/-}$ mice with female C57BL/6 mouse breeders. F1 $Snca^{-/+}$ mice were bred to *Snca*-knockout ($Snca^{-/-}$) mice to make F2 heterozygotes and knockout mice. Other F1 ($Snca^{-/+}$) mice were backcrossed to sibling heterozygotes to obtain sibling pairs from each genotype. The *Snca* genotypes were verified by the protocol described above using tail snip analysis. All animal use was reviewed and approved by the local IACUC and institutional biosafety committee prior to the initiation of the experiments. For encephalitis disease analysis, animals were weighed upon randomized selection of both male and female mice from each treatment group. Following subcutaneous (s.c.) or intracerebral (i.c.) inoculation, mice were monitored at least twice daily for signs of disease and weight loss. Animals exhibiting advanced encephalitis signs (extreme lethargy, seizures, paralysis, no response to the toe pinch test) and animals exhibiting a >15% loss of weight from their weight at enrollment were sacrificed.

Caspase-3 activity assays. Caspase-3 activity assays were completed as previously described (31). Briefly, whole-brain lysates were made from individual cortical or striatal tissue specimens. Whole-brain lysate was immediately analyzed for caspase-3 activity following harvest and sample preparation using a caspase-3 fluorometric assay kit (R&D systems) per the manufacturer's instructions.

HEK293T cell transfection assays. HEK293T cells (CRL-3216; ATCC) were maintained at 37°C in 5% CO_2 in Dulbecco's modified Eagle medium supplemented with 1% penicillin-streptomycin, 10% heat-inactivated fetal bovine serum, 1% HEPES, and 1% sodium pyruvate. Plasmid 40822 EGFP-alphasynuclein-WT was obtained from Addgene. The experimental plasmid and an empty vector control plasmid were transfected into HEK293T cells using the Fugene HD transfection reagent according to the manufacturer's instructions (Promega). Additional experiments were performed using polyethylenimine (PEI) for transfection, but there was no change in efficiency from that achieved with Fugene HD, so Fugene HD was used for subsequent experiments.

Statistical analysis. All data were analyzed using Prism (version 6) software (GraphPad Prism) and the analysis for each data set indicated below. Prior to the animal studies, a power analysis was performed to determine the sample size needed for the detection of a 10-fold difference between groups with an alpha value of 0.05. Animals were randomly assigned to treatment groups using a random-number generator. Both male and female mice were used at random.

RESULTS

We first determined if WNV infection of primary cultured neurons altered the expression of the Asyn protein. Using a neuroinvasive WNV isolate (NY99; MOI, 1), we inoculated primary mouse striatal neurons and determined the level of Asyn protein expression over time (Fig. 1). Primary striatal neurons were prepared and virus was inoculated as previously described (30). At 12 and 24 h postinoculation, the level of striatal neuron expression of the Asyn protein increased by 2-fold compared to that for the mock-infected control ($P = 0.086$, analysis of variance [ANOVA]; Fig. 1A and B). Given that WNV induced Asyn expression in cultured neurons, we evaluated brain tissue from patients with acute WNV encephalitis for Asyn expression using an Olympus VS120 fluorescence slide-scanning microscope with an OrcaR2 high-resolution imaging system. We assayed brain tissue from uninfected patients (control), WNV-infected subcortical gray matter, and WNV-infected white matter (Table 1). Since WNV does not infect white matter, analysis of this region served as an additional internal control for Asyn expression levels. The subcortical gray matter of patients with WNV encephalitis (cerebral spinal fluid positive for IgM to WNV) exhibited an increased mean fluorescence intensity of Asyn compared to control patients and white matter regions of WNV-infected patients (Fig. 1C and D). Asyn expression was increased in brain regions, such as the basal ganglia, that also expressed WNV envelope antigen and that had increased virus-induced injury, as measured by determination of the amount of cleaved caspase-3 (Fig. 1E).

Since WNV infection was associated with increased Asyn protein expression in primary neurons and in the brains of humans with encephalitis, we investigated the effects of Asyn expression on WNV growth and pathogenesis in neurons and in a mouse model of WNV encephalitis as previously described (29, 30, 32). We obtained *Snca*$^{-/-}$ mice (The Jackson Laboratory) and bred them with wild-type C57BL/6 mice with an *Snca*$^{+/+}$ genotype to make F1 *Snca*$^{-/+}$ mice. The F1 *Snca*$^{-/+}$ mice were backcrossed to sibling pairs to produce F2 mice representing all genotypes: *Snca*$^{+/+}$, *Snca*$^{-/+}$, and *Snca*$^{-/-}$ mice. F2 sibling pairs were used for experiments. Adult mice (age, 10 weeks) of each genotype were inoculated with WNV (NY99, 10^3 PFU by subcutaneous [s.c.] footpad injection) and sacrificed at day 8 postinoculation for analysis of WNV growth and WNV-induced injury and morbidity. While 8 days is a relatively early time point, this was used due to the increased mortality of knockout mice after that period of time. After perfusion, the brains were separated anatomically into cortical and striatal brain tissue for WNV titer analysis. At 8 days postinoculation, *Snca*$^{-/-}$ mice exhibited a mean increase of $10^{4.5}$ viral particles/g brain tissue ($P = 0.0001$, ANOVA with the Kruskal-Wallis test) in the striatum ($1.3 \times 10^7 \pm 4.12 \times 10^6$ PFU/g) and cortex ($2.1 \times 10^7 \pm 8.6 \times 10^6$ PFU/g) compared to the mean viral titers in the striatum ($2.6 \times 10^2 \pm 1.6 \times 10^2$ PFU/g) and cortex ($4.1 \times 10^2 \pm 1.8 \times 10^2$ PFU/g) of *Snca*$^{-/+}$ mice and the striatum ($1 \times 10^2 \pm 6.8$ PFU/g) and cortex ($3.3 \times 10^2 \pm 2.3 \times 10^2$ PFU/g) of *Snca*$^{+/+}$ mice (Fig. 2A). Additional *Snca*$^{-/+}$ and *Snca*$^{-/-}$ mice were inoculated with WNV as described above and sacrificed at day 4 postinoculation. There was no consistent evidence of increased viral growth in the brains of *Snca*$^{-/-}$ mice compared to that in the brains of *Snca*$^{-/+}$ mice at an earlier time point, 4 days after infection (Fig. 2B). Thus, there was no significant or consistent evidence of increased neuroinvasion at day 4 postinfection in the absence of Asyn expression. In addition to brain tissue, we also evaluated spleen tissue in assays for viral growth in the above-described groups. There was no significant difference in the viral titers in the spleens of *Snca*$^{-/+}$ and *Snca*$^{-/-}$ mice at day 4 or day 8

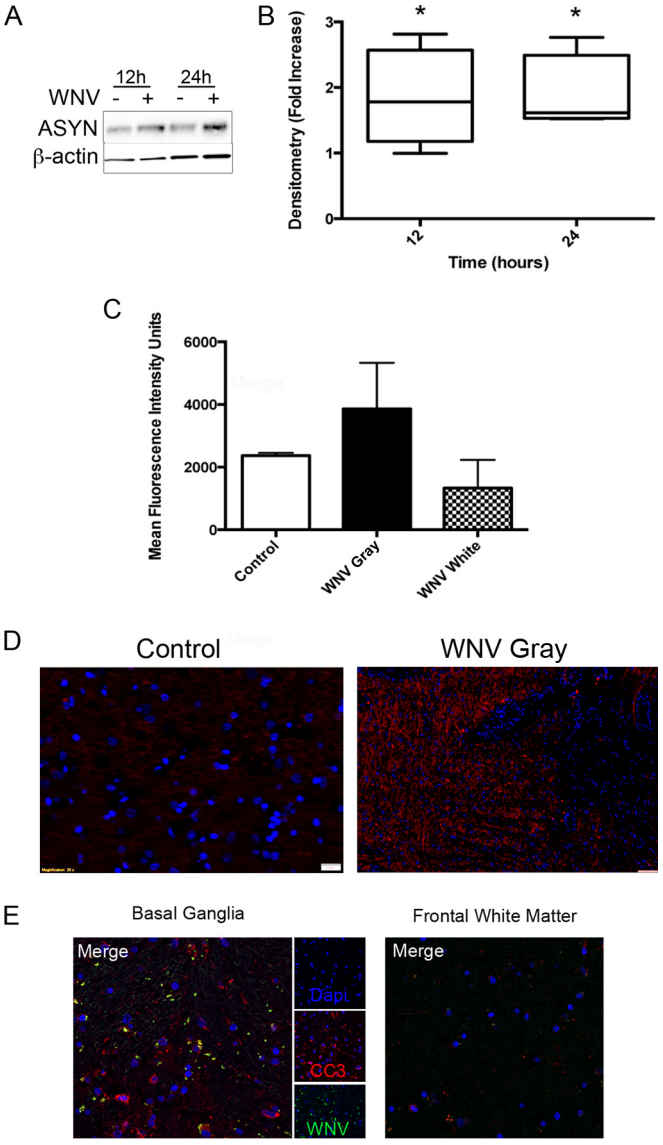

FIG 1 West Nile virus infection increases alpha-synuclein expression. (A) Western blot analysis of WNV-inoculated primary striatal neurons using antibody to Asyn at the indicated time points. (B) Densitometry analysis from Western blots for Asyn using primary striatal neurons from WNV-inoculated *Snca*$^{+/+}$ mice in three replicate experiments. Data are shown as the mean ± SEM fold increase in band density compared to that for the mock-inoculated control and corrected for β-actin loading. *, $P = 0.086$, nonparametric ANOVA. (C) Mean fluorescence intensity units of immunolabeled Asyn expression in brain tissue from uninfected control patients and tissue from patients with WNV encephalitis. Samples from subcortical gray matter (WNV Gray) and white matter regions (WNV white) were also included. Error bars represent the SEMs of the means obtained from the patients listed in Table 1. (D) Asyn expression (Cy3, red) in formalin-fixed, paraffin-embedded sections from autopsy brain tissue consisting of basal ganglia (WNV Gray) from a patient with WNV encephalitis and basal ganglia from an uninfected patient (Control). Magnification, ×200; bar = 50 μm. (E) Laser confocal images from IF analysis of human brain tissue infected with WNV showing the distribution and colocalization of WNV envelope antigen (FITC, green) and CC3 (Cy3, red). Magnifications, ×400.

TABLE 1 Patient data for brain samples obtained for analysis whose results are shown in Fig. 1

Age (yr)	Sex[a]	WNV infection status	Cause of death	Immune status
66	M	Positive	Encephalitis	Immune competent
46	F	Positive	Encephalitis	Immunosuppressed
63	M	Positive	Cardiac arrest	Immune competent
57	F	Positive	Encephalitis	Immunosuppressed
56	M	Negative	Interstitial pneumonia	Immune competent
70	M	Negative	Esophageal carcinoma	Immune competent

[a] M, male; F, female.

postinoculation (Fig. 2C). Three of the four *Snca*$^{-/-}$ mice infected with WNV exhibited spleen WNV titers below the limit of detection at day 8 postinfection (Fig. 2C). However, all of the *Snca*$^{-/-}$ mice exhibited high viral loads in the CNS. Since Asyn is nearly exclusively expressed in neurons, these data verified that inhibition of viral growth by Asyn is specific to neurons.

We also determined whether increased viral growth in the brains of WNV-inoculated *Snca*$^{-/-}$ mice resulted in a change in mortality. *Snca*$^{+/+}$, *Snca*$^{-/+}$, and *Snca*$^{-/-}$ mice were inoculated with WNV (10^3 PFU s.c.) and followed for signs of encephalitis. All mice were sacrificed upon development of advanced signs of encephalitis or a weight loss of >15% of their enrollment body weight. Mice of each genotype were inoculated and followed for disease signs without knowledge of the genotype. The genotype was determined after the experiment was completed. WNV-inoculated *Snca*$^{-/-}$ mice exhibited a significantly ($P < 0.0001$, log-rank test) increased mortality rate (95%) compared to that for WNV-inoculated *Snca*$^{-/+}$ mice (20%) and *Snca*$^{+/+}$ mice (25%) (Fig. 2D and E). Following WNV inoculation, *Snca*$^{-/-}$ mice exhibited a median survival of 10 days (hazard ratio [HR], 10.1; 95% confidence interval [CI], 3.89 to 21.5), whereas the median length of survival for *Snca*$^{-/+}$ and *Snca*$^{+/+}$ mice was undefined due to prolonged survival at the end of the study (HR, 0.1; 95% CI, 0.05 to 0.25; Fig. 2D and E). Next, we determined the effect of Asyn expression on WNV RNA levels in the brain using qRT-PCR of striatal brain tissue from infected animals as described above. WNV-inoculated *Snca*$^{-/-}$ mice exhibited a mean 9.4-fold increase in viral RNA replication compared to WNV-inoculated *Snca*$^{-/+}$ mice (Fig. 2F). Taken together, these data suggest that Asyn expression inhibits viral growth and replication, resulting in increased mortality in knockout mice.

To define the role of Asyn in virus-induced neuronal injury, we utilized primary cortical neuronal cultures as previously described (29, 30). Additionally, we created a new model of WNV infection in primary mouse striatal neurons and compared viral growth, infectivity, and injury in these two neuronal subtypes in culture. Following WNV infection (MOI, 1) of cortical and striatal neurons, we found that WNV growth in cortical neurons was relatively restricted compared to that in striatal neurons ($P = 0.0045$, two-way ANOVA; Fig. 3A). Next, we inoculated striatal and cortical primary neurons with WNV (MOI, 1) and at 24 h postinfection, we immunolabeled the cells with antibodies to DARP32 (a

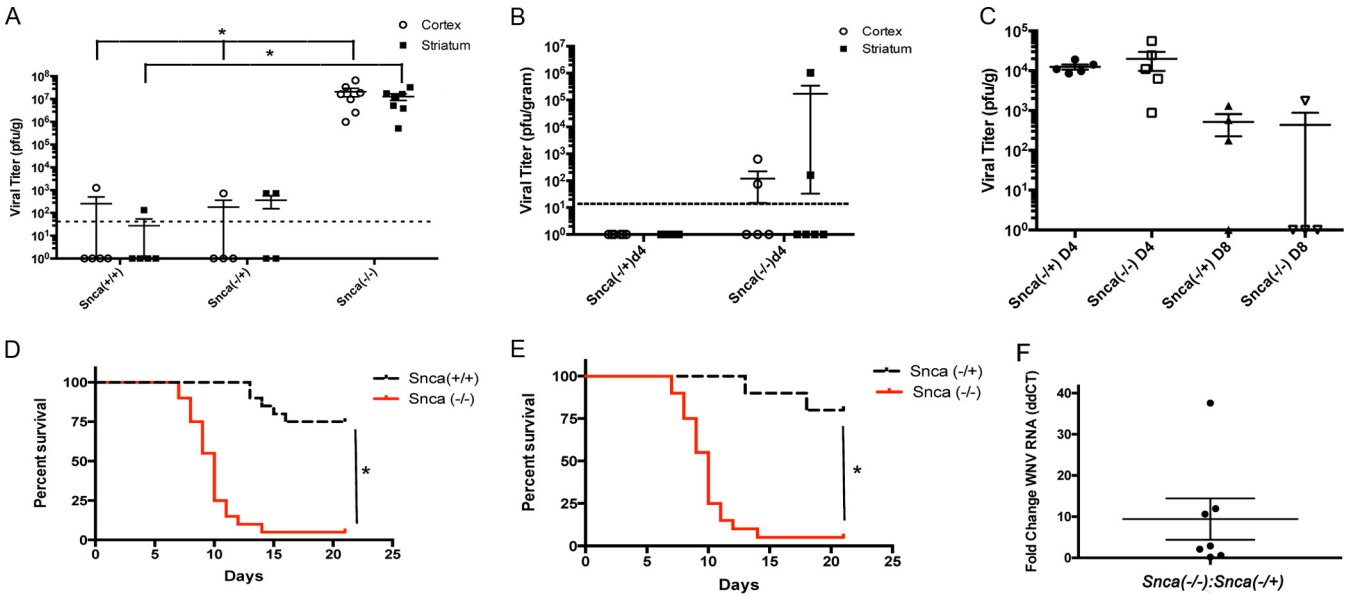

FIG 2 Alpha-synuclein expression inhibits WNV growth and disease in the CNS. (A) Viral titers in striatal and cortical brain tissue from WNV-inoculated (NY99, 10^3 PFU s.c.) mice in the indicated groups and brain sections at day 8 postinoculation. Dotted line, limit of detection. *, $P = 0.0001$. Each data point represents an individual. (B) Viral titers in striatal and cortical brain tissue from WNV-inoculated (NY99, 10^3 PFU s.c.) mice in the indicated groups at day 4 (d4) postinoculation. Dotted line, limit of detection. (C) Spleens from *Snca*$^{-/+}$ and *Snca*$^{-/-}$ mice that were sacrificed at day 4 (D4) and day 8 (D8) postinoculation were analyzed for the infectious viral titer. No significant difference in the spleen viral titer was detected between the groups. (D and E) Survival analysis following WNV inoculation (10^3 PFU s.c.) of *Snca*$^{-/-}$ mice and comparison of survival of *Snca*$^{-/-}$ mice to that of *Snca*$^{+/+}$ mice (D) and *Snca*$^{-/+}$ mice (E). *, $P < 0.0001$. Data for the same group of *Snca*$^{-/-}$ mice ($n = 20$) are represented in both panels D and E and were individually compared to those for *Snca*$^{+/+}$ ($n = 20$) and *Snca*$^{-/+}$ ($n = 10$) mice. (F) Fold change in WNV RNA replication, determined using qRT-PCR, in striatal brain tissue from WNV-infected *Snca*$^{-/-}$ mice compared to that in striatal brain tissue from *Snca*$^{-/+}$ mice. RNA isolated from the same groups was used for the viral titer assays at day 8 postinfection. The mean fold increase was 9.4 ± 5.02 (SEM). ddCT, $\Delta\Delta C_T$, where C_T represents the threshold cycle.

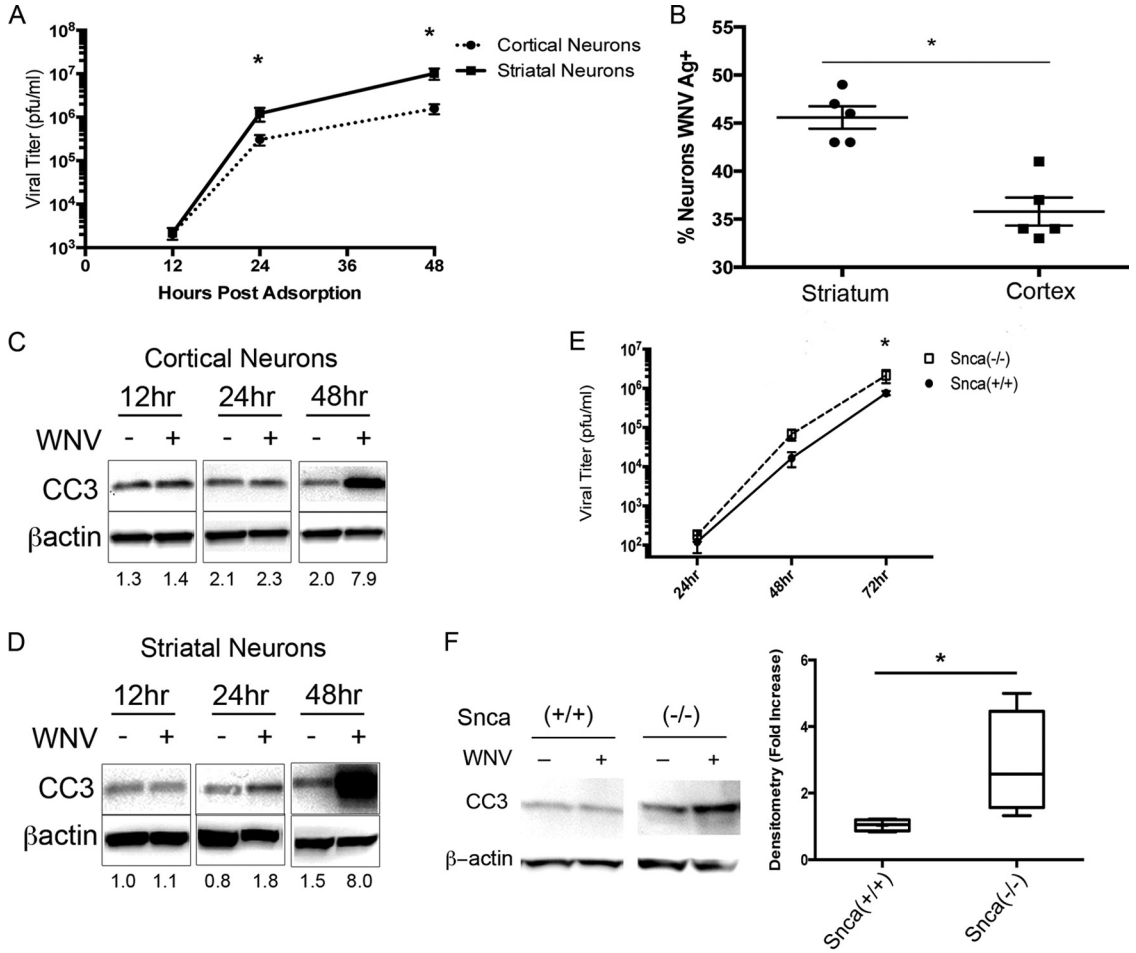

FIG 3 Alpha-synuclein expression modulates WNV-induced caspase-3 activation in primary cortical neurons. (A) Primary mouse cortical and striatal neuron cultures were inoculated with WNV (MOI, 1), and the infectious viral titer in the supernatant was determined at the indicated time points postinoculation. *, $P = 0.0045$. (B) Primary neurons were made from the striatal and cortical tissues, inoculated with WNV (MOI, 1), and harvested at 24 h postinoculation for determination of WNV infectivity using immunocytochemistry and cell counts for cells double positive for the WNV envelope antigen (Ag^+) and DARP32 (a striatal neuron marker) or Emx1 (a cortical neuron marker). *, $P = 0.009$. (C and D) Representative images of Western blots of whole-cell lysates probed for CC3 from WNV-inoculated (MOI, 1) primary cortical neurons (C) and primary striatal neurons (D) harvested at the indicated times postinoculation. The values for densitometry below each band are the mean values from three independent experiments. (E) WNV infectious titer in supernatants from $Snca^{+/+}$ and $Snca^{-/-}$ primary cortical neurons assayed at the indicated time points postinoculation with WNV (MOI, 0.001). Data are for 5 experimental replicates per treatment group. *, $P < 0.05$, two-way ANOVA with multiple comparisons. (F) (Left) Representative Western blot analysis for CC3 in primary cortical neurons from $Snca^{+/+}$ and $Snca^{-/-}$ mice performed at 24 h postinoculation with WNV (MOI, 1). (Right) Densitometry analysis from Western blots for CC3 performed at 24 h postinfection. Data are the mean ± SEM fold increase from three replicate experiments with WNV-inoculated primary cortical neurons from $Snca^{-/-}$ mice (2.6 ± 0.8) and wild-type mice (1.05 ± 0.08). The data are shown as the mean fold increase in density compared to that for the mock-inoculated control and were corrected for β-actin loading. *, $P = 0.03$.

striatal neuron marker) or Emx1 (a cortical neuron marker) and colabeled the cells for WNV envelope protein. Using immunocytochemistry analysis and confocal microscopy, we counted the number of infected neurons (WNV envelope positive) in each neuron population and found that neurons derived from the cortex (Emx1 positive) exhibited consistently decreased infection rates (35.8% ± 1.5% [standard error of the mean {SEM}]) in culture compared to neurons derived from the striatum (DARP32 positive, 45.6% ± 1.2% [SEM]; $P = 0.0009$, unpaired t test with the Welch correction; Fig. 3B). Given the relative resistance of primary cortical neurons to viral infection compared to that of striatal neurons, we next evaluated differences in virus-induced injury, as measured by the level of cleaved caspase-3 (CC3) expression. Following inoculation with WNV (MOI, 1), we found that primary cortical neurons expressed increased amounts of CC3 by 48 h postinoculation (Fig. 3C); however, primary striatal neurons expressed increased amounts of CC3 as early as 24 h postinoculation (Fig. 3D). Since cortical neurons exhibited increased resistance to viral growth and injury, we determined if Asyn expression contributed to this resistance to viral infection in primary cortical neurons. We made primary cortical neurons from $Snca^{+/+}$ and $Snca^{-/-}$ mice. Primary neurons were inoculated with WNV (MOI, 0.001), and the infectious viral titer in the supernatant was determined at the time points indicated in Fig. 3E. We found that at 72 h postinoculation the WNV titer in the cortical neurons from $Snca^{-/-}$ mice was significantly ($P < 0.05$, two-way ANOVA with Sidak's multiple-comparison test) increased compared to that in the cortical neurons from $Snca^{+/+}$ mice (mean difference, 1.39 ×

10^6 PFU/ml; 95% CI, 2.6×10^6 to 2.1×10^5 PFU/ml; Fig. 3E). Next, we defined the role of Asyn in the virus-induced injury of cortical neurons by inoculating wild-type and Asyn-knockout mouse primary cortical neurons with WNV (MOI, 1). At 24 h postinoculation, when the results were compared as the fold increase in activity from that in mock-inoculated mice, the cortical neurons from WNV-inoculated (MOI, 1) *Snca*$^{-/-}$ mice exhibited significantly ($P = 0.03$, Mann-Whitney test) increased levels of CC3 expression compared with the primary cortical neurons from WNV-inoculated *Snca*$^{+/+}$ mice (2.6-fold and 1.05-fold, respectively; Fig. 3F). Thus, Asyn expression protects primary cortical neurons from WNV growth and injury in culture.

Next, we determined the role of Asyn expression in virus-induced neuronal injury using an animal model of WNV encephalitis. *Snca*$^{-/+}$ and *Snca*$^{-/-}$ mice were mock inoculated or inoculated with WNV (10^3 PFU s.c.) and sacrificed for analysis at day 8 postinoculation. At day 8 postinoculation, on immunohistochemistry analysis, brain tissue from WNV-infected *Snca*$^{-/-}$ mice exhibited a significant increase in CC3 expression compared to brain tissue from WNV-inoculated *Snca*$^{-/+}$ and *Snca*$^{+/+}$ control mice (Fig. 4A). To better quantify this response, we completed 3 experimental replicates with the same mice described above following WNV infection, with 2 to 3 mice being used in each group per experiment on the basis of the availability of mice from the different breeding groups. At day 8 postinoculation, the mice were sacrificed and brain tissue from the cortex and striatum were harvested for caspase-3 activity assays. When the results were compared as the fold change in activity from that in mock-inoculated mice, WNV-inoculated *Snca*$^{-/-}$ mice exhibited significantly increased CC3 activity in the cortex (7.3-fold ± 2.4-fold [SEM]) and striatum (4.6-fold ± 0.8-fold [SEM]) compared to striatal brain tissue from *Snca*$^{-/+}$ mice (1.25-fold ± 0.5-fold [SEM]) (*, $P = 0.007$, ANOVA with the Kruskal-Wallis test; Fig. 4B). These data suggest that Asyn expression protects the brain as well as primary neurons from virus-induced injury.

Using a neuroinvasive WNV strain, we found that Asyn expression inhibited the growth of infectious viral particles in the brain. We next used a vaccine strain of an alphavirus, Venezuelan equine encephalitis virus (VEEV; strain TC83), to determine if Asyn expression inhibits the growth of virus from a different enveloped RNA virus family not related to WNV (33). *Snca*$^{-/-}$ and *Snca*$^{-/+}$ mice were inoculated with VEEV TC83 in the footpad (10^7 PFU) and sacrificed at day 8 postinoculation, and the brain tissue viral titer was determined. Viral growth in striatal tissue ($4.7 \times 10^7 \pm 4.7 \times 10^7$ PFU/g [SEM]) and cortical tissue ($2.5 \times 10^8 \pm 1.6 \times 10^8$ PFU/g [SEM]) from TC83-infected *Snca*$^{-/-}$ mice was significantly ($P = 0.03$, ANOVA with the Mann-Whitney test) increased compared with that in striatal and cortical tissue from *Snca*$^{-/+}$ mice, in which virus was undetectable (Fig. 5A). Next, *Snca*$^{-/-}$ and *Snca*$^{-/+}$ mice were inoculated with VEEV TC83 (10^7 PFU s.c.) as described above and monitored for signs of encephalitis and weight loss. VEEV TC83-inoculated *Snca*$^{-/-}$ mice exhibited a trend toward less weight gain after day 8 postinoculation compared to that for VEEV TC83-inoculated *Snca*$^{-/+}$ mice (Fig. 5B). Next, *Snca*$^{-/-}$ and *Snca*$^{-/+}$ mice were inoculated by intracerebral injection (10^3 PFU of VEEV TC83) and monitored for weight loss and morbidity from encephalitis. Following i.c. inoculation of VEEV TC83, *Snca*$^{-/-}$ mice exhibited a significantly ($P = 0.04$, unpaired t test) increased weight loss (mean weight change, −14.8%) compared to that for *Snca*$^{-/+}$ mice (mean weight change, +0.4%) (Fig. 5C). One *Snca*$^{-/-}$ mouse i.c. infected with TC83 was sacrificed due to weight loss of >15% of its initial body weight, per the enrollment criteria (Fig. 5D). None of the survivors to the end of the study period at 14 days postinoculation had detectable virus in the brain.

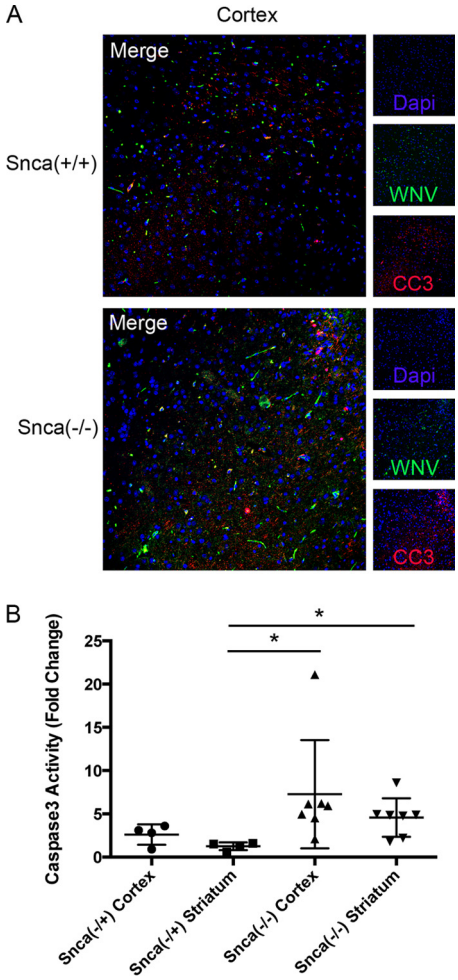

FIG 4 Asyn expression prevents WNV-induced caspase-3 activation in the brain. (A) Representative IFA image of cortical brain tissue from WNV-inoculated *Snca*$^{+/+}$ and *Snca*$^{-/-}$ mice at day 8 postinoculation. Brain tissue was immunolabeled with antibodies to the WNV envelope (FITC, green) and cleaved caspase-3 (Cy3, red). Images representative of those from 6 replicates are shown. Dapi, 4′,6-diamidino-2-phenylindole. Magnification, ×600. (B) Caspase-3 activity assay values obtained from individual mice and for the indicated brain regions of the indicated groups at day 8 postinoculation with WNV (NY99, 10^3 PFU s.c.). Values are expressed as the fold change compared to the value for mock-inoculated control animals in the same groups harvested in parallel. *, $P = 0.007$. The mean ± SEM fold increases in CC3 activity for the *Snca*$^{-/+}$ mouse cortex (2.6 ± 0.59), the *Snca*$^{-/+}$ mouse striatum (1.25 ± 0.23), the *Snca*$^{-/-}$ mouse cortex (7.3 ± 2.4), and the *Snca*$^{-/-}$ mouse striatum (4.6 ± 0.84) found at day 8 postinfection with WNV are provided.

Our data show that *Snca* expression inhibits enveloped RNA virus growth and disease in the CNS. In primary cortical neurons from Asyn-knockout mice, we found evidence that Asyn expression alters neuron survival and viral growth. These data imply that Asyn may alter viral pathogenesis within the neuron. Asyn is known to localize with Rab1$^+$ vesicles, alter ER membrane trafficking, and modulate ER stress signaling (27). Flaviviruses are

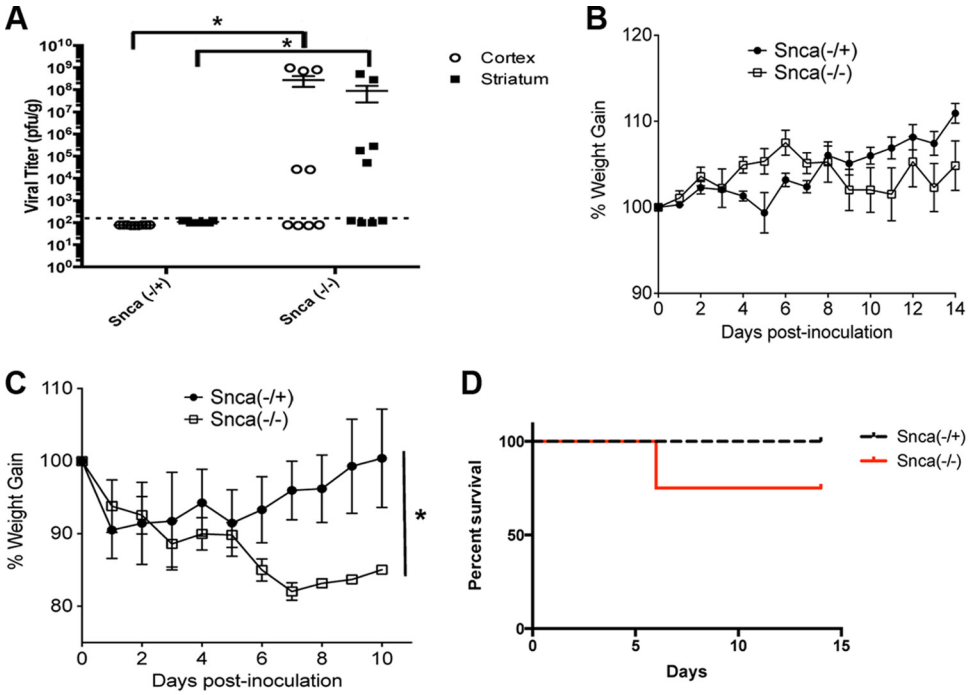

FIG 5 Alpha-synuclein expression inhibits VEEV TC83 growth in the CNS. (A) Infectious viral titers in striatal and cortical brain tissue from VEEV TC83-inoculated (10^7 PFU s.c.) mice in the indicated groups at day 7 postinoculation. Dotted line, limit of detection. *, $P = 0.03$. (B) Mean percent weight change over time in VEEV TC83-inoculated (10^7 PFU s.c.) mice in the indicated groups ($n = 11$). (C) Mean percent weight change over time in VEEV TC83-inoculated (10^3 PFU, i.c. injection) mice in the indicated groups. *, $P = 0.04$ ($n = 4$ per group). (D) Percent survival over time of VEEV TC83-inoculated (10^3 PFU i.c.) mice in the indicated groups ($n = 4$ per group).

also known to increase ER stress signaling in support of viral replication and growth (34, 35). Since both flaviviruses (e.g., WNV) and alphaviruses (e.g., VEEV) utilize ER-derived membrane systems for virus replication, we analyzed the interactions between WNV and neuronal membrane compartments. Primary striatal neurons were mock inoculated or inoculated with WNV (MOI, 1) and harvested at 24 h postinoculation for immunofluorescence analysis (IFA) of WNV envelope (Env) protein (FITC, green) and Asyn (Cy3, red) expression. In primary striatal neuron cultures, the WNV Env protein colocalized with Asyn in perinuclear regions of infected neurons (Fig. 6A and B). Since WNV replication occurs in ER-derived membranes in the perinuclear region of cells, we determined the localization of WNV-induced Asyn to membrane compartments. Both cortical and striatal primary neuronal cultures were mock inoculated or inoculated with WNV (MOI, 1) and harvested for IFA at 24 h postinoculation. We found evidence of significantly ($P < 0.0001$, two-tailed, unpaired t test) increased colocalization between Rab1 and Asyn in WNV-infected cortical neurons (58.04% ± 4.7% of neurons [SEM]) compared to that in mock-inoculated cortical neurons (6.7% ± 2.2% of neurons [SEM]) (Fig. 6D and E). We also found a significant ($P = 0.01$, two-tailed, unpaired t test) increase in colocalization between Rab1 and Asyn following WNV infection in primary striatal neurons (26.9% ± 6.1% of neurons [SEM]) compared to that in mock-inoculated, primary striatal neurons (4.96% ± 1.5% of neurons) (Fig. 6F and G). Using the same groups described above, we also evaluated WNV-induced Asyn localization with $Rab5^+$ membranes and $Rab7^+$ membranes and found no change in localization with infection (data not shown). Thus, WNV-induced Asyn localizes to the perinuclear regions of $Rab1^+$ membranes in neurons that are positive for WNV proteins.

Prior studies have shown that Asyn localizes to $Rab1^+$ membranes, alters membrane trafficking, and modulates ER stress signaling (27, 36). Given that WNV manipulates ER stress signaling (34, 37, 38), we hypothesized that Asyn expression modulates ER stress signaling following viral infection and that, in the absence of Asyn, ER stress signals are increased in support of WNV replication. To evaluate this hypothesis, we inoculated primary striatal neuron cultures with WNV (MOI, 1) as described above and harvested neurons at 24 h postinoculation for ER stress protein analysis using Western blotting. Mock- and WNV-inoculated primary striatal neurons from $Snca^{-/-}$ mice exhibited significantly increased levels of expression of PERK, phospho-eIF2α, Ero1L-1α, protein disulfide isomerase (PDI), and Atf6 compared to the mean levels for matched mock- and WNV-inoculated primary striatal neurons from $Snca^{+/+}$ mice (Fig. 7). Other ER stress signals, including IRE1α and calnexin (data not shown), did not exhibit changes in protein expression in association with Asyn expression. These data support the hypothesis that Asyn expression modulates ER stress signaling events that are associated with WNV replication and growth and WNV-induced apoptosis.

We localized WNV-induced Asyn to $Rab1^+$ membranes. These membrane compartments are associated with ER membrane trafficking and cellular protein exocytosis. Since protein exocytosis is required for some innate immune signaling events, we determined the effect of Asyn expression on the expression of select innate immune proteins in the brains of WNV-infected mice. $Snca^{+/+}$, $Snca^{-/+}$, and $Snca^{-/-}$ mice were inoculated with

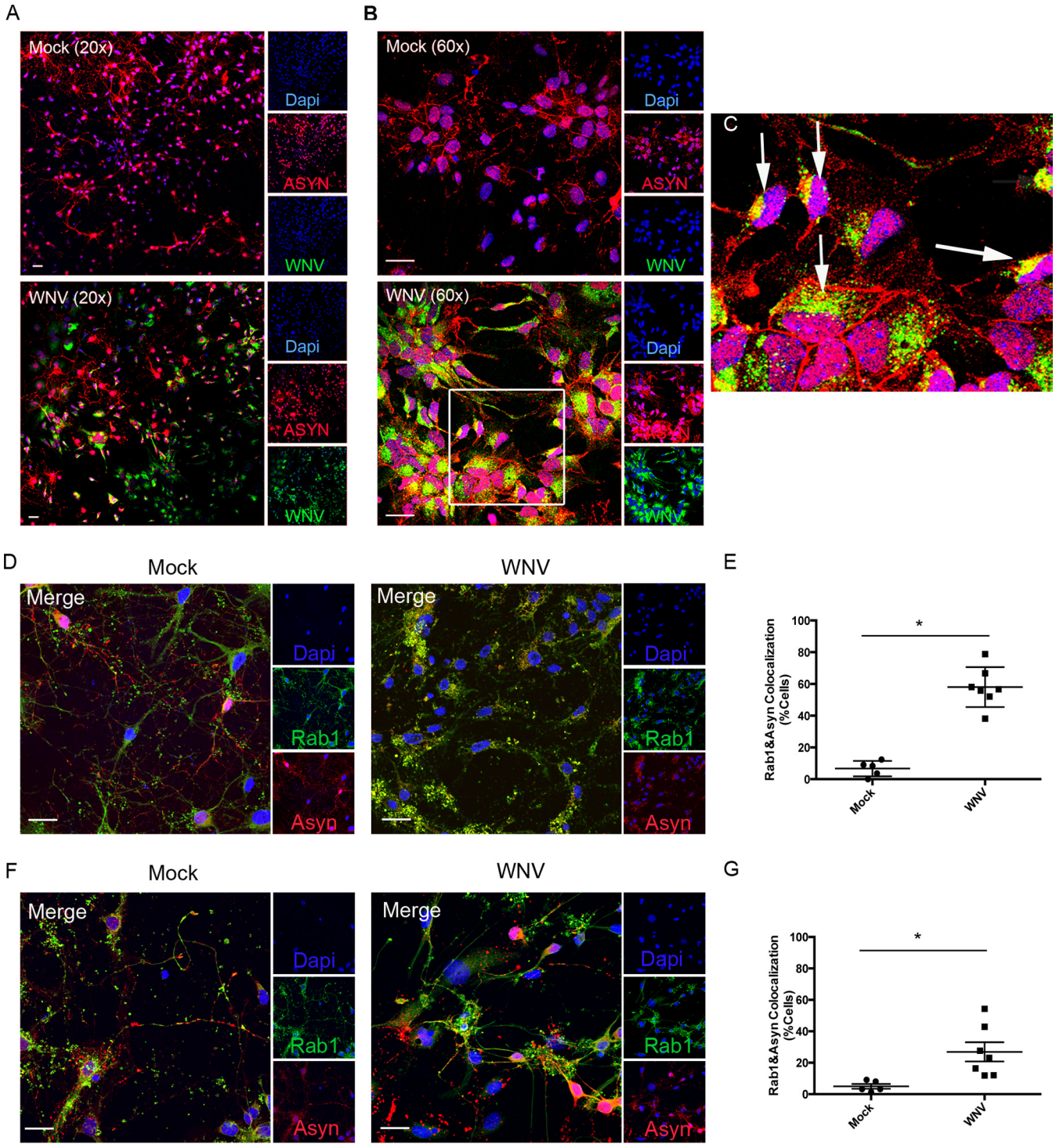

FIG 6 Alpha-synuclein localizes with the WNV envelope antigen and Rab1-positive membranes. (A and B) IFA images of mock and WNV-inoculated (MOI, 1) primary striatal neurons obtained using antibodies to the WNV envelope (FITC, green) and alpha-synuclein (Cy3, red). Bars = 25 μm. The data are representative of those from three replicate experiments. (C) Digitally magnified image of the boxed area in panel B showing the subcellular localization of Asyn (Cy3, red) and the WNV envelope (FITC, green) antigen. Magnification, ×1,000. Arrows, red-green colocalization in the perinuclear regions of infected neurons. (D to G) Primary cortical neurons (D and E) and primary striatal neurons (F and G) from *Snca*$^{+/+}$ mice following mock or WNV inoculation (MOI, 1). Neurons were harvested at 24 h postinoculation for IFA of the indicated proteins. Quantification of the percentage of primary cortical neurons (*, $P < 0.0001$) (E) and primary striatal neurons (*, $P = 0.01$) (G) exhibiting Asyn-Rab1 colocalization following mock or WNV inoculation, as described above. Data are for three experimental replicates per group. Each dot represents the mean of individual values from the three experiments. Bars = 25 μm.

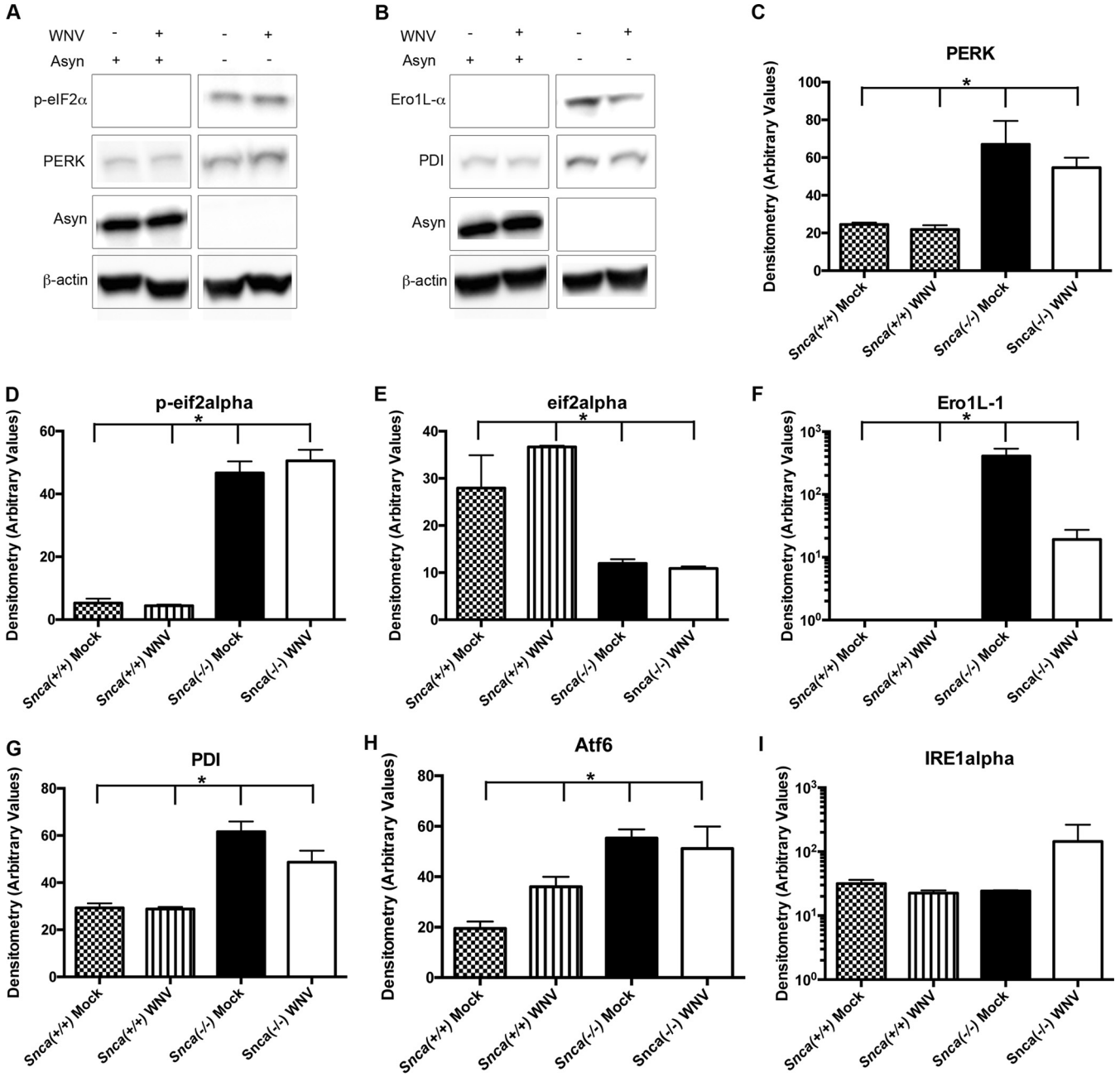

FIG 7 Asyn expression modulates ER stress signaling. Primary cortical neurons derived from *Snca*$^{+/+}$ and *Snca*$^{-/-}$ mice were mock inoculated or inoculated with WNV (MOI, 1) and harvested at 24 h for Western blot analysis of whole-cell lysates for ER stress signaling proteins. (A) Representative image of a Western blot probed with antibodies to phosphorylated eIF2alpha (p-eIF2alpha), PERK, Asyn, and β-actin. (B) Representative image of a Western blot probed with antibodies to Ero1L-1α, PDI, Asyn, and β-actin. Data are for three experimental replicates. (C to I) Semiquantitative densitometry analysis of mean band density corrected for by the density of β-actin for PERK (*, $P = 0.006$) (C), phospho-eIF2α (p-eIF2α; *, $P = 0.011$) (D), total eIF2α (*, $P = 0.001$) (E), Ero1L-1α (*, $P = 0.0006$) (F), PDI (*, $P = 0.003$) (G), Atf6 (*, $P = 0.013$) (H), and IRE1α ($P = 0.2$, no significant difference) (I). Data were obtained from three experimental replicates, and means were compared using a nonparametric ANOVA with the Kruskal-Wallis test.

WNV (10^3 PFU s.c. in the footpad), and brain tissue was harvested at day 8 postinoculation for protein analysis. Whole-tissue lysates from the cortex and striatal tissue were analyzed, using ELISA, for the expression of TNF-α, interleukin-6 (IL-6), interferon alpha, and interferon beta. We found no significant changes in the levels of expression of TNF-α, IL-6, interferon alpha, or interferon beta following WNV infection when mice expressing Asyn and Asyn-knockout mice were compared (Fig. 8). As expected, following WNV infection we did find evidence of significantly increased expression of IL-6 ($P = 0.04$) and interferon beta ($P = 0.05$) in the brain tissue of mice expressing Asyn and Asyn-knockout mice compared to that in the brain tissue of mock-inoculated mice. These data suggest that Asyn expression restricts viral infection independently of the pro-

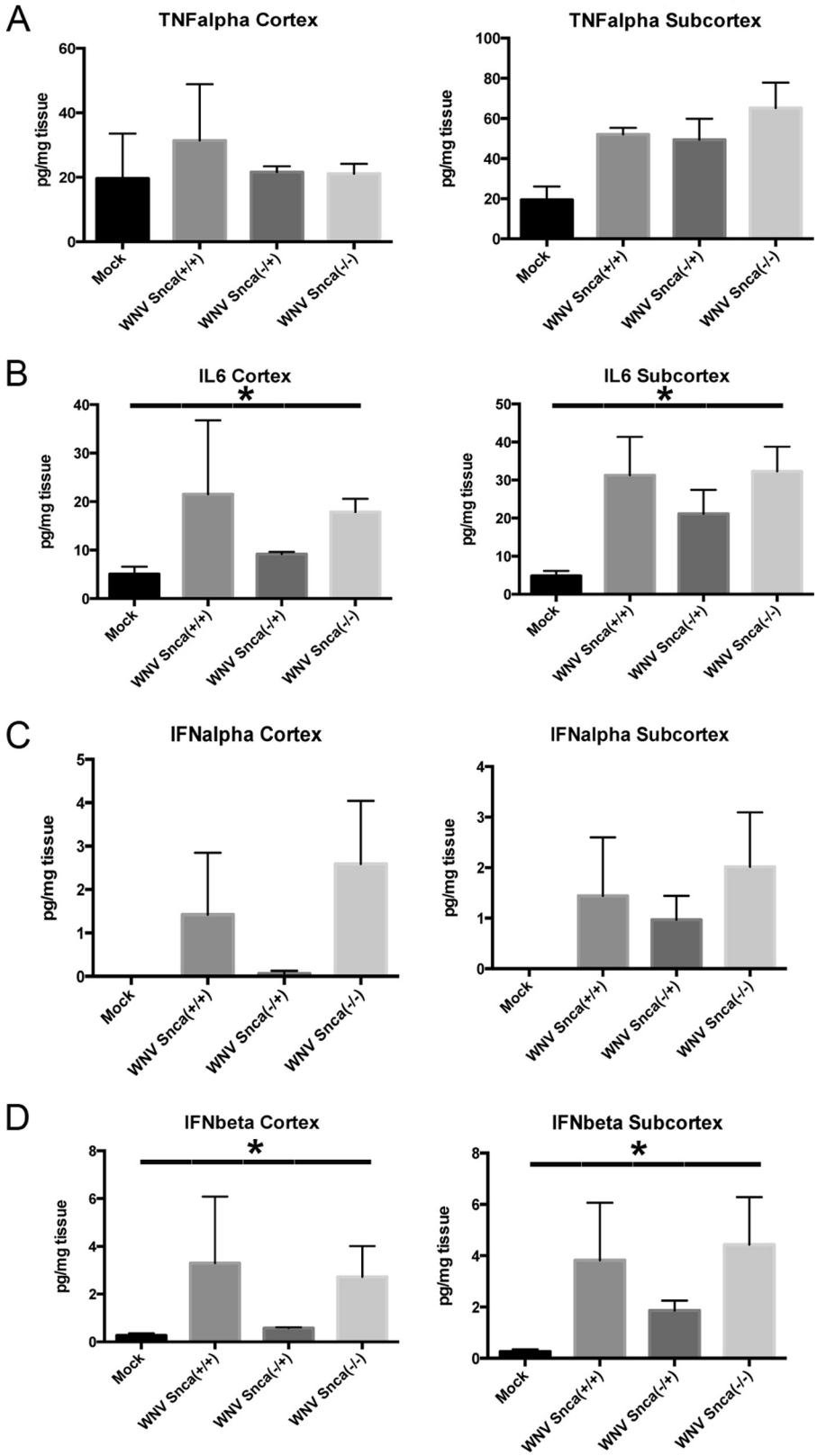

FIG 8 Asyn expression does not alter WNV-induced TNF-α, IL-6, or interferon production. Brain tissue was harvested from the indicated regions at day 8 postinoculation with WNV (10^3 PFU s.c. footpad) to obtain tissue lysates. Following quantification of total protein concentrations, ELISAs for TNF-α (A), IL-6 (*, $P = 0.04$) (B), interferon alpha (C), and interferon beta (*, $P = 0.05$) (D) were completed. Data are for three replicates per treatment group, and the mean and SEM for each group are shown.

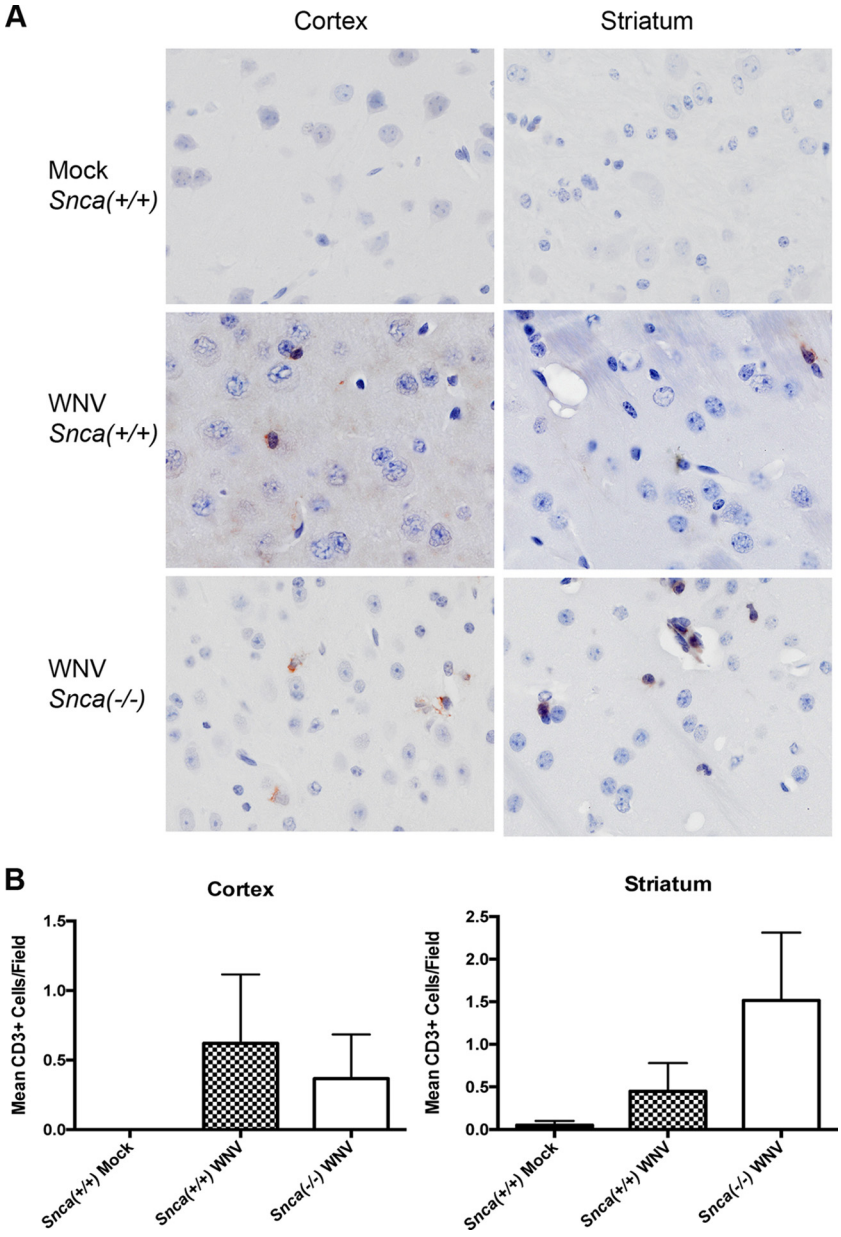

FIG 9 Asyn expression does not alter $CD3^+$ cell infiltration into the brains of WNV-infected mice. Perfused brain tissue from the indicated regions was harvested at day 8 postinoculation with WNV (10^3 PFU s.c. footpad) or after mock inoculation and paraffin embedded for immunohistochemistry analysis. Tissue was immunolabeled with antibody to CD3, labeled with NovaRed peroxidase as the secondary antibody, and counterstained using hematoxylin. (A) Representative images of the indicated brain regions from mock-inoculated $Snca^{+/+}$ mice and WNV-inoculated $Snca^{+/+}$ and $Snca^{-/-}$ mice. Magnification, ×600. (B) $CD3^+$ cell counts per high-power field in the indicated brain regions and groups determined by an observer blind to the results. Mean $CD3^+$ counts ± SEM are displayed.

duction of these selected innate immune responses associated with interferon.

While WNV-inoculated neurons may produce similar levels of select innate immune signals, we next determined if lymphocyte responses were altered by expression of Asyn. $Snca^{+/+}$ and $Snca^{-/-}$ mice were inoculated with WNV (10^3 PFU s.c. in the footpad), and brain tissue was harvested at day 8 postinoculation for immunohistochemistry analysis for $CD3^+$ cells. There were no significant differences in $CD3^+$ cell infiltration into $Snca^{+/+}$ and $Snca^{-/-}$ mouse brains following WNV infection (Fig. 9). These data show that Asyn expression did not quantitatively alter T-cell infiltration into brain tissue following WNV infection.

Asyn forms multimers on intracellular membranes, and multimerization is thought to be related to the intraneuronal functions of native Asyn expression (25). We have shown that WNV infection increased Asyn protein expression. Next, we determined whether viral infection increased the multimerization of Asyn on neuronal membranes in primary striatal neuronal cultures. Primary striatal neurons were isolated from $Snca^{+/+}$ mice and inoculated with WNV (MOI, 1). At 24 h postinoculation, neuronal

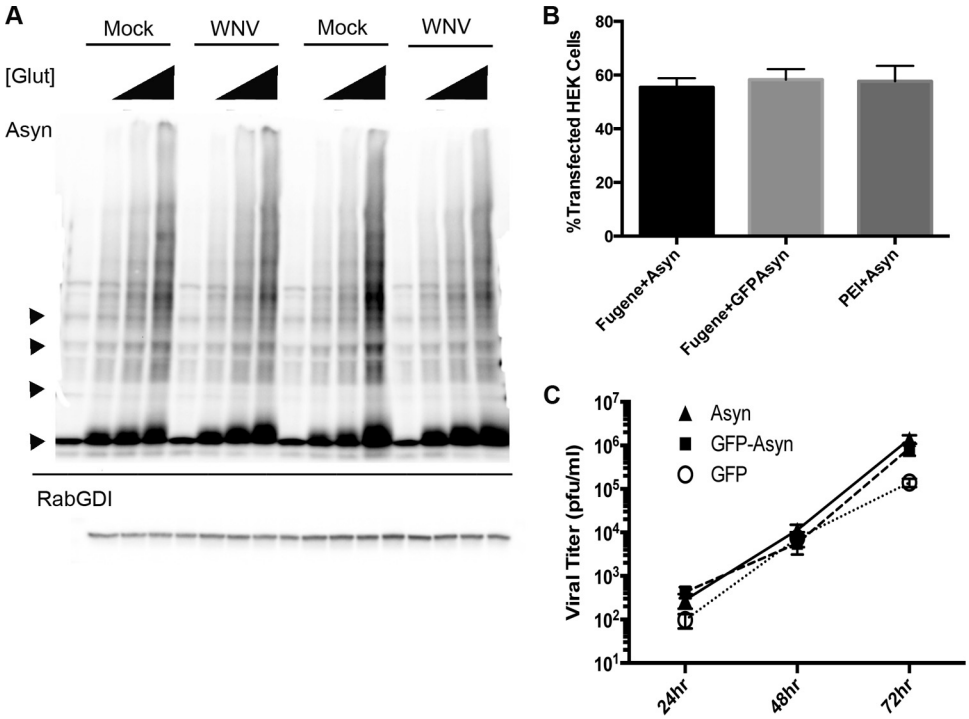

FIG 10 WNV does not alter Asyn multimers in primary striatal neuron cultures. Primary striatal neurons were mock or WNV inoculated (MOI, 1) and treated with glutaraldehyde (Glut) at concentrations of 0%, 0.00125%, 0.0025%, or 0.005% upon harvesting at 24 h postinoculation. (A) Representative image of a Western blot obtained with a whole neuronal lysate labeled with antibody to Asyn. Each Western blot was also probed for Rab-GDI as a control for a cellular protein that does not cross-link. The image is representative of the images from three experimental replicates. Triangles on the left of the blot, expected molecular weights of the Asyn monomer, dimer, trimer, and tetramer (from bottom to top, respectively). (B) HEK293T cells were transfected with a plasmid expressing Asyn or green fluorescent protein (GFP)-Asyn. A mean ± SEM transfection efficiency of from 55 to 58% was calculated using IF analysis and antibody to Asyn or green fluorescent protein. Cells were analyzed at 24 h posttransfection, and means from 11 experimental replicates were calculated. PEI, polyethylenimine transfection reagent; Fugene, Fugene HD transfection reagent. (C) HEK293T cells were transfected with plasmids expressing green fluorescent protein alone, Asyn alone, or green fluorescent protein and Asyn. At 24 h posttransfection, cells were inoculated with WNV (MOI, 0.001) and the viral titer in the supernatants was determined at the indicated time points ($n = 6$ experimental replicates per treatment group).

lysates were incubated with increasing concentrations of glutaraldehyde and analyzed by Western blotting. Following WNV infection, we found no evidence of increased multimerization of Asyn in primary striatal neurons (Fig. 10A). We next wanted to evaluate multimerization in an Asyn expression system and so transfected HEK293T cells with plasmids expressing Asyn. First, we determined if Asyn expression altered WNV growth in this nonneuronal cell type. We optimized plasmid-mediated Asyn expression in HEK293T cells and calculated the transfection efficiency to be a mean of 57% of cells (Fig. 10B). At 24 h after transfection, cells were inoculated with WNV (MOI, 0.001) and the viral titer in the supernatants was determined at the time points indicated in Fig. 10C. We found no evidence of Asyn-dependent restriction of viral growth in Asyn-transfected HEK293T cells (Fig. 10C). These data support our data with mice that show Asyn-dependent restriction of viral infection is specific to neurons. Since there was no effect on viral growth in this system, we did not proceed further to evaluate multimer formation in transfected HEK293T cells.

DISCUSSION

We have discovered a novel, native function for Asyn expression in the brain. Our data show that Asyn can function as a novel restriction factor for RNA virus infections in neurons. Following viral infection, Asyn expression was increased in primary neurons and in tissue samples from patients with acute WNV encephalitis. In Asyn-knockout mice, the WNV infectious titer in the brain was increased 5 orders of magnitude and the rate of WNV-induced mortality was dramatically increased. To extend these findings to another family of RNA viruses that cause CNS disease, we evaluated the pathogenesis of VEEV, an encephalitic alphavirus, in Asyn-knockout mice. We used an attenuated strain of VEEV (TC83) that cannot escape IFIT1 restriction (33). Using VEEV TC83, we found that the virus grew to titers of up to 10^8 PFU per gram of brain tissue in the brains of Asyn-knockout mice, and Asyn-knockout mice experienced significant disease from VEEV TC83, as evidenced by increased weight loss compared to that found in TC83-inoculated *Snca*$^{-/+}$ mice. These data show that Asyn inhibits CNS disease and viral growth in very distinct RNA viruses.

Given that increased viral growth and accelerated morbidity and mortality were seen in Asyn-knockout mice, we determined whether Asyn-knockout mice exhibited changes in virus-induced caspase-3 activation. Virus-induced caspase-3 activation is known to be a primary mechanism of virus-induced neuronal death in the central nervous system (31, 39). We found that primary cortical neurons were relatively resistant to WNV growth and WNV-induced injury compared to primary striatal neurons. With the knockout of Asyn, cortical neurons expressed increased amounts of virus-induced CC3 at much earlier time points following infec-

tion. These data suggest that Asyn plays a role in modulating cell death in neurons following viral infection. These data were validated in the mouse model of WNV encephalitis. Analysis of caspase-3 activity in the brains of WNV-infected Asyn-knockout mice revealed that it was significantly increased compared to that in the brains of control mice. Thus, we concluded that Asyn expression protects mice from viral growth and virus-induced neuronal injury. We next determined the mechanism of Asyn-dependent inhibition of viral infection.

Given this pattern of inhibition, we investigated possible mechanisms that may contribute to Asyn-dependent inhibition within the neuron. The role of native Asyn expression in neurons has been extensively studied, given the etiologic role of Asyn in the development of Parkinson's disease (40). The Asyn structure is closely related to its membrane-associated functions, and it localizes to membrane-trafficking vesicles in the perinuclear regions of the neuron and in the synapse (24, 41, 42). In the neuronal soma, Asyn localizes to ER-derived Rab1$^+$ vesicles to inhibit ER-to-Golgi body transport, resulting in the modulation of ER stress signaling (27, 43). So, we evaluated the localization of virus-induced Asyn within the neuron. We found that virus-induced Asyn localized with viral envelope proteins and significantly increased the localization with Rab1$^+$ membranes.

Previous work has shown that Asyn localization to Rab1$^+$ membranes alters membrane transport from the ER to the Golgi body, resulting in changes in ER stress signals and ER remodeling within the neuron (27, 36). In general, positive-stranded RNA viruses are dependent on membrane remodeling to support viral replication. Flaviviruses are known to manipulate ER stress signaling in support of viral replication (34–37), so we determined the role of Asyn expression on ER stress signaling responses. We discovered significant increases in specific ER stress signals in Asyn-knockout primary neurons. The levels of PERK, phosphorylated eIF2alpha, Ero1L-1α, PDI, and Atf6 expression were all significantly increased in Asyn-knockout primary cortical neurons. Atf6 was previously shown to support Kunjin virus replication by modulating innate immune responses (37). West Nile virus and dengue virus are known to modulate ER stress signals, such as eIF2α and PERK expression, in support of viral growth and to modulate apoptotic signaling (34, 35). We also found it interesting that our screen exhibited marked increases in both Ero1L-1α and PDI expression. Ero1L-1α is an ER-associated protein that oxidizes PDI, which can directly catalyze the formation of disulfide bonds in folding proteins (44). The members of the PDI family of proteins act as enzymatic chaperones in the ER for misfolded proteins and can mediate apoptosis signaling through a Bak-dependent proapoptotic function (45). In the absence of Asyn expression, the activation of specific ER stress pathways identified in this system would be expected to support viral growth, support viral replication, and modulate apoptotic signaling. These data explain in part the increased viral growth and increased apoptosis following viral infection of Asyn-knockout cortical neurons.

Since virus-induced Asyn was localized to Rab1$^+$ membrane-trafficking vesicles, we determined if Asyn expression altered the release of innate immune signaling proteins. Our data show that the loss of Asyn had no significant effect on some aspects of the innate immune response; thus, the loss of important innate responses is not likely the mechanism for the dramatic increase in viral growth following viral infection of Asyn-knockout mice. Additionally, Asyn-knockout mice exhibited spleen titers of WNV that were similar to or lower than the spleen titers exhibited by control mice. Thus, Asyn expression does not alter the expression of innate immune signaling proteins and does not alter peripheral viral replication. Since CD3$^+$ cells are vital to controlling WNV infection in the brain (46), we determined if Asyn expression altered lymphocyte infiltration into the brain following viral infection. We found no quantitative difference in T-cell infiltration in the absence of Asyn expression that would explain the increased viral growth and injury in virus-infected Asyn-knockout mice. Other effects of Asyn on surrounding cell types will need to be explored in the future.

Our work has focused on the native function of Asyn, and we did not address the role of Lewy bodies (LBs), which are predominantly composed of Asyn. Since LBs are not seen in acute WNV infection (5), we did not investigate the role of LB formation during acute viral pathogenesis, but the role of LBs in viral pathogenesis remains an important question and an area of active interest in our laboratories. Recently, Asyn was shown to form multimers on membranes that may be related to its native function (25). We evaluated the role of WNV infection in the formation of Asyn multimers in primary striatal neurons. We found no evidence of increased multimer formation following viral infection. To extend these studies, we transfected HEK293T cells with Asyn to develop a cell culture system that we could easily manipulate in order to study the role of Asyn gene sequences on viral restriction and possible multimer formation. While we obtained good transfection rates, this system did not recapitulate the neuronal phenotype. These data are consistent with the findings obtained with our mouse model of WNV infection. In Asyn-knockout mice, we found no change in viral growth in nonneuronal tissues, such as the spleen. Thus, the role of Asyn in the inhibition of viral infection seems to be specific to neurons.

This work defines a novel antiviral restriction factor and provides the first clear evidence for an antiviral function of natively expressed Asyn in neurons. This work raises several important and intriguing questions. Since Asyn is constitutively expressed in neurons, it is unlikely to have evolved to restrict only RNA virus infections of neurons. Additional studies into the role of Asyn expression in the restriction of common human alphaherpesviruses, such as herpes simplex virus or varicella-zoster virus, are needed. Both of these viruses are known to undergo latency in neurons and to have very high seroprevalence rates in human populations. If Asyn evolved in vertebrates to inhibit neuroinvasive viral infection, then it should restrict herpesvirus infections in the CNS. Additionally, viral infections may act as an environmental trigger for the misfolding of Asyn over time and initiate the prion-like spread of Asyn to the CNS in genetically susceptible individuals. This is currently an active area of study within the laboratory. Lastly, we started these studies with the idea that Asyn may be acutely toxic following viral infection and found quite the opposite. Our data imply that the acute onset of Parkinsonian features during WNV encephalitis is likely due to the virus-induced death of dopaminergic neurons, resulting in the acute loss of dopamine signaling. Taken together, our data provide significant insight into the pathogenesis of acute viral infections in the brain and provide a novel, native function for Asyn expression in the CNS.

ACKNOWLEDGMENTS

J.D.B. is supported by a University of Colorado SOM Neuroscience Center Pilot Award and Department of Medicine Funds. T.E.M. is supported by NIAID grant R01AI108725. K.D.S. is supported by a University of Colorado T32 microbiology training grant.

We thank Michael Diamond for providing VEEV TC83 for our studies and thank Bette K. Kleinschmidt-DeMasters at University of Colorado Hospital Pathology Department for helping to obtain and provide human tissue samples for analysis. We also thank the Colorado Clinical & Translational Sciences Institute for core laboratory support and the Light Imaging Core.

FUNDING INFORMATION

University of Colorado Anschutz Medical Campus Center for Neuroscience provided funding to J. David Beckham. University of Colorado Department of Medicine provided funding to J. David Beckham. NIH/NIAID provided funding to Thomas E. Morrison under grant number R01AI108725.

REFERENCES

1. **Beckham JD, Tyler KL.** 2012. Neuro-intensive care of patients with acute CNS infections. Neurotherapeutics **9:**124–138. http://dx.doi.org/10.1007/s13311-011-0086-5.
2. **Carrera JP, Forrester N, Wang E, Vittor AY, Haddow AD, Lopez-Verges S, Abadia I, Castano E, Sosa N, Baez C, Estripeaut D, Diaz Y, Beltran D, Cisneros J, Cedeno HG, Travassos da Rosa AP, Hernandez H, Martinez-Torres AO, Tesh RB, Weaver SC.** 2013. Eastern equine encephalitis in Latin America. N Engl J Med **369:**732–744. http://dx.doi.org/10.1056/NEJMoa1212628.
3. **Solomon T.** 2004. Flavivirus encephalitis. N Engl J Med **351:**370–378. http://dx.doi.org/10.1056/NEJMra030476.
4. **Ali M, Safriel Y, Sohi J, Llave A, Weathers S.** 2005. West Nile virus infection: MR imaging findings in the nervous system. AJNR Am J Neuroradiol **26:**289–297.
5. **Armah HB, Wang G, Omalu BI, Tesh RB, Gyure KA, Chute DJ, Smith RD, Dulai P, Vinters HV, Kleinschmidt-DeMasters BK, Wiley CA.** 2007. Systemic distribution of West Nile virus infection: postmortem immunohistochemical study of six cases. Brain Pathol **17:**354–362. http://dx.doi.org/10.1111/j.1750-3639.2007.00080.x.
6. **Tyler KL, Pape J, Goody RJ, Corkill M, Kleinschmidt-DeMasters BK.** 2006. CSF findings in 250 patients with serologically confirmed West Nile virus meningitis and encephalitis. Neurology **66:**361–365. http://dx.doi.org/10.1212/01.wnl.0000195890.70898.1f.
7. **Sejvar JJ, Haddad MB, Tierney BC, Campbell GL, Marfin AA, Van Gerpen JA, Fleischauer A, Leis AA, Stokic DS, Petersen LR.** 2003. Neurologic manifestations and outcome of West Nile virus infection. JAMA **290:**511–515. http://dx.doi.org/10.1001/jama.290.4.511.
8. **Jang H, Boltz D, Sturm-Ramirez K, Shepherd KR, Jiao Y, Webster R, Smeyne RJ.** 2009. Highly pathogenic H5N1 influenza virus can enter the central nervous system and induce neuroinflammation and neurodegeneration. Proc Natl Acad Sci U S A **106:**14063–14068. http://dx.doi.org/10.1073/pnas.0900096106.
9. **Jang H, Boltz DA, Webster RG, Smeyne RJ.** 2009. Viral parkinsonism. Biochim Biophys Acta **1792:**714–721. http://dx.doi.org/10.1016/j.bbadis.2008.08.001.
10. **Cho H, Proll SC, Szretter KJ, Katze MG, Gale M, Jr, Diamond MS.** 2013. Differential innate immune response programs in neuronal subtypes determine susceptibility to infection in the brain by positive-stranded RNA viruses. Nat Med **19:**458–464. http://dx.doi.org/10.1038/nm.3108.
11. **Forman MS, Trojanowski JQ, Lee VM.** 2004. Neurodegenerative diseases: a decade of discoveries paves the way for therapeutic breakthroughs. Nat Med **10:**1055–1063. http://dx.doi.org/10.1038/nm1113.
12. **Vila M, Przedborski S.** 2004. Genetic clues to the pathogenesis of Parkinson's disease. Nat Med **10**(Suppl):S58–S62.
13. **Spillantini MG, Crowther RA, Jakes R, Hasegawa M, Goedert M.** 1998. Alpha-synuclein in filamentous inclusions of Lewy bodies from Parkinson's disease and dementia with Lewy bodies. Proc Natl Acad Sci U S A **95:**6469–6473. http://dx.doi.org/10.1073/pnas.95.11.6469.
14. **Chartier-Harlin MC, Kachergus J, Roumier C, Mouroux V, Douay X, Lincoln S, Levecque C, Larvor L, Andrieux J, Hulihan M, Waucquier N, Defebvre L, Amouyel P, Farrer M, Destee A.** 2004. Alpha-synuclein locus duplication as a cause of familial Parkinson's disease. Lancet **364:**1167–1169. http://dx.doi.org/10.1016/S0140-6736(04)17103-1.
15. **Ibanez P, Bonnet AM, Debarges B, Lohmann E, Tison F, Pollak P, Agid Y, Durr A, Brice A.** 2004. Causal relation between alpha-synuclein gene duplication and familial Parkinson's disease. Lancet **364:**1169–1171. http://dx.doi.org/10.1016/S0140-6736(04)17104-3.
16. **Kruger R, Kuhn W, Muller T, Woitalla D, Graeber M, Kosel S, Przuntek H, Epplen JT, Schols L, Riess O.** 1998. Ala30Pro mutation in the gene encoding alpha-synuclein in Parkinson's disease. Nat Genet **18:**106–108. http://dx.doi.org/10.1038/ng0298-106.
17. **Polymeropoulos MH, Lavedan C, Leroy E, Ide SE, Dehejia A, Dutra A, Pike B, Root H, Rubenstein J, Boyer R, Stenroos ES, Chandrasekharappa S, Athanassiadou A, Papapetropoulos T, Johnson WG, Lazzarini AM, Duvoisin RC, Di Iorio G, Golbe LI, Nussbaum RL.** 1997. Mutation in the alpha-synuclein gene identified in families with Parkinson's disease. Science **276:**2045–2047. http://dx.doi.org/10.1126/science.276.5321.2045.
18. **Singleton AB, Farrer M, Johnson J, Singleton A, Hague S, Kachergus J, Hulihan M, Peuralinna T, Dutra A, Nussbaum R, Lincoln S, Crawley A, Hanson M, Maraganore D, Adler C, Cookson MR, Muenter M, Baptista M, Miller D, Blancato J, Hardy J, Gwinn-Hardy K.** 2003. Alpha-synuclein locus triplication causes Parkinson's disease. Science **302:**841. http://dx.doi.org/10.1126/science.1090278.
19. **Tan EK, Chai A, Teo YY, Zhao Y, Tan C, Shen H, Chandran VR, Teoh ML, Yih Y, Pavanni R, Wong MC, Puvan K, Lo YL, Yap E.** 2004. Alpha-synuclein haplotypes implicated in risk of Parkinson's disease. Neurology **62:**128–131. http://dx.doi.org/10.1212/01.WNL.0000101721.25345.DC.
20. **Zarranz JJ, Alegre J, Gomez-Esteban JC, Lezcano E, Ros R, Ampuero I, Vidal L, Hoenicka J, Rodriguez O, Atares B, Llorens V, Gomez Tortosa E, del Ser T, Munoz DG, de Yebenes JG.** 2004. The new mutation, E46K, of alpha-synuclein causes Parkinson and Lewy body dementia. Ann Neurol **55:**164–173. http://dx.doi.org/10.1002/ana.10795.
21. **Masliah E, Rockenstein E, Veinbergs I, Mallory M, Hashimoto M, Takeda A, Sagara Y, Sisk A, Mucke L.** 2000. Dopaminergic loss and inclusion body formation in alpha-synuclein mice: implications for neurodegenerative disorders. Science **287:**1265–1269. http://dx.doi.org/10.1126/science.287.5456.1265.
22. **Abeliovich A, Schmitz Y, Farinas I, Choi-Lundberg D, Ho WH, Castillo PE, Shinsky N, Verdugo JM, Armanini M, Ryan A, Hynes M, Phillips H, Sulzer D, Rosenthal A.** 2000. Mice lacking alpha-synuclein display functional deficits in the nigrostriatal dopamine system. Neuron **25:**239–252. http://dx.doi.org/10.1016/S0896-6273(00)80886-7.
23. **Dauer W, Kholodilov N, Vila M, Trillat AC, Goodchild R, Larsen KE, Staal R, Tieu K, Schmitz Y, Yuan CA, Rocha M, Jackson-Lewis V, Hersch S, Sulzer D, Przedborski S, Burke R, Hen R.** 2002. Resistance of alpha-synuclein null mice to the Parkinsonian neurotoxin MPTP. Proc Natl Acad Sci U S A **99:**14524–14529. http://dx.doi.org/10.1073/pnas.172514599.
24. **Burre J, Sharma M, Tsetsenis T, Buchman V, Etherton MR, Sudhof TC.** 2010. Alpha-synuclein promotes SNARE-complex assembly in vivo and in vitro. Science **329:**1663–1667. http://dx.doi.org/10.1126/science.1195227.
25. **Burre J, Sharma M, Sudhof TC.** 2014. Alpha-synuclein assembles into higher-order multimers upon membrane binding to promote SNARE complex formation. Proc Natl Acad Sci U S A **111:**E4274–E4283. http://dx.doi.org/10.1073/pnas.1416598111.
26. **Auluck PK, Caraveo G, Lindquist S.** 2010. Alpha-synuclein: membrane interactions and toxicity in Parkinson's disease. Annu Rev Cell Dev Biol **26:**211–233. http://dx.doi.org/10.1146/annurev.cellbio.042308.113313.
27. **Cooper AA, Gitler AD, Cashikar A, Haynes CM, Hill KJ, Bhullar B, Liu K, Xu K, Strathearn KE, Liu F, Cao S, Caldwell KA, Caldwell GA, Marsischky G, Kolodner RD, Labaer J, Rochet JC, Bonini NM, Lindquist S.** 2006. Alpha-synuclein blocks ER-Golgi traffic and Rab1 rescues neuron loss in Parkinson's models. Science **313:**324–328. http://dx.doi.org/10.1126/science.1129462.
28. **National Research Council.** 2011. Guide for the care and use of laboratory animals, 8th ed. National Academies Press, Washington, DC.
29. **Beatman E, Oyer R, Shives KD, Hedman K, Brault AC, Tyler KL, Beckham JD.** 2012. West Nile virus growth is independent of autophagy activation. Virology **433:**262–272. http://dx.doi.org/10.1016/j.virol.2012.08.016.

30. **Shives KD, Beatman EL, Chamanian M, O'Brien C, Hobson-Peters J, Beckham JD.** 2014. West Nile virus-induced activation of mammalian target of rapamycin complex 1 supports viral growth and viral protein expression. J Virol **88:**9458–9471. http://dx.doi.org/10.1128/JVI.01323-14.
31. **Beckham JD, Tuttle KD, Tyler KL.** 2010. Caspase-3 activation is required for reovirus-induced encephalitis in vivo. J Neurovirol **16:**306–317. http://dx.doi.org/10.3109/13550284.2010.499890.
32. **Clarke P, Leser JS, Quick ED, Dionne KR, Beckham JD, Tyler KL.** 2014. Death receptor-mediated apoptotic signaling is activated in the brain following infection with West Nile virus in the absence of a peripheral immune response. J Virol **88:**1080–1089. http://dx.doi.org/10.1128/JVI.02944-13.
33. **Hyde JL, Gardner CL, Kimura T, White JP, Liu G, Trobaugh DW, Huang C, Tonelli M, Paessler S, Takeda K, Klimstra WB, Amarasinghe GK, Diamond MS.** 2014. A viral RNA structural element alters host recognition of nonself RNA. Science **343:**783–787. http://dx.doi.org/10.1126/science.1248465.
34. **Ambrose RL, Mackenzie JM.** 2011. West Nile virus differentially modulates the unfolded protein response to facilitate replication and immune evasion. J Virol **85:**2723–2732. http://dx.doi.org/10.1128/JVI.02050-10.
35. **Pena J, Harris E.** 2011. Dengue virus modulates the unfolded protein response in a time-dependent manner. J Biol Chem **286:**14226–14236. http://dx.doi.org/10.1074/jbc.M111.222703.
36. **Colla E, Coune P, Liu Y, Pletnikova O, Troncoso JC, Iwatsubo T, Schneider BL, Lee MK.** 2012. Endoplasmic reticulum stress is important for the manifestations of alpha-synucleinopathy in vivo. J Neurosci **32:**3306–3320. http://dx.doi.org/10.1523/JNEUROSCI.5367-11.2012.
37. **Ambrose RL, Mackenzie JM.** 2013. ATF6 signaling is required for efficient West Nile virus replication by promoting cell survival and inhibition of innate immune responses. J Virol **87:**2206–2214. http://dx.doi.org/10.1128/JVI.02097-12.
38. **Schuck S, Prinz WA, Thorn KS, Voss C, Walter P.** 2009. Membrane expansion alleviates endoplasmic reticulum stress independently of the unfolded protein response. J Cell Biol **187:**525–536. http://dx.doi.org/10.1083/jcb.200907074.
39. **Samuel MA, Morrey JD, Diamond MS.** 2007. Caspase 3-dependent cell death of neurons contributes to the pathogenesis of West Nile virus encephalitis. J Virol **81:**2614–2623. http://dx.doi.org/10.1128/JVI.02311-06.
40. **Bendor JT, Logan TP, Edwards RH.** 2013. The function of alpha-synuclein. Neuron **79:**1044–1066. http://dx.doi.org/10.1016/j.neuron.2013.09.004.
41. **Boassa D, Berlanga ML, Yang MA, Terada M, Hu J, Bushong EA, Hwang M, Masliah E, George JM, Ellisman MH.** 2013. Mapping the subcellular distribution of alpha-synuclein in neurons using genetically encoded probes for correlated light and electron microscopy: implications for Parkinson's disease pathogenesis. J Neurosci **33:**2605–2615. http://dx.doi.org/10.1523/JNEUROSCI.2898-12.2013.
42. **Sharma M, Burre J, Sudhof TC.** 2011. CSPalpha promotes SNARE-complex assembly by chaperoning SNAP-25 during synaptic activity. Nat Cell Biol **13:**30–39. http://dx.doi.org/10.1038/ncb2131.
43. **Thayanidhi N, Helm JR, Nycz DC, Bentley M, Liang Y, Hay JC.** 2010. Alpha-synuclein delays endoplasmic reticulum (ER)-to-Golgi transport in mammalian cells by antagonizing ER/Golgi SNAREs. Mol Biol Cell **21:**1850–1863. http://dx.doi.org/10.1091/mbc.E09-09-0801.
44. **Enyedi B, Varnai P, Geiszt M.** 2010. Redox state of the endoplasmic reticulum is controlled by Ero1L-alpha and intraluminal calcium. Antioxid Redox Signal **13:**721–729. http://dx.doi.org/10.1089/ars.2009.2880.
45. **Zhao G, Lu H, Li C.** 2015. Proapoptotic activities of protein disulfide isomerase (PDI) and PDIA3 protein, a role of the Bcl-2 protein Bak. J Biol Chem **290:**8949–8963. http://dx.doi.org/10.1074/jbc.M114.619353.
46. **Sitati EM, Diamond MS.** 2006. $CD4^+$ T-cell responses are required for clearance of West Nile virus from the central nervous system. J Virol **80:**12060–12069. http://dx.doi.org/10.1128/JVI.01650-06.